JMEPEG
https://doi.org/10.1007/s11665-026-15323-7

©ASM International
1059-9495/$19.00

ORIGINAL RESEARCH ARTICLE

Comparative Tribological, Tribocorrosion, and Thermomechanical Performance of Electron Beam Physical Vapor Deposition Yttria-Stabilized Zirconia and Calcia-Stabilized Zirconia Coatings on SR34 Steel for Top Piston Ring Applications

Uthirapathy Chandrasekaran, K. Hariharan, Saravanan Raju, and C. Ilamvazhuthi

Submitted: 19 April 2026 / Revised: 4 September 2026 / Accepted: 15 September 2026

Yttria-stabilized zirconia (YSZ) and calcia-stabilized zirconia (CSZ) were deposited on SR34 steel by electron beam physical vapor deposition (EB-PVD) as potential top piston ring coatings for internal combustion engines. The study aimed to enhance the surface, tribological, and tribocorrosion behavior of SR34 steel in extreme service environments. The deposited layers were characterized for microstructure, phase formation, surface roughness, microhardness, sliding wear, abrasion resistance, thermal expansion behavior, and tribocorrosion behavior. SEM/EDS analysis confirmed the formation of continuous, adherent ceramic coatings, with measured thicknesses of approximately 1.35 μm for the YSZ coating and 1.16 μm for the CSZ coating. The surface roughness decreased to 0.235 μm and 0.188 μm for YSZ and CSZ, respectively, compared with 0.274 μm for the uncoated SR34. The coatings had significantly higher microhardness (614.54 HV for CSZ and 668.54 HV for YSZ) than the 390.4 HV substrate, with YSZ showing the highest hardness. Pin-on-disk tests on cast iron showed that both coating types significantly reduced wear loss, wear rate, and coefficient of friction relative to the uncoated substrate, with CSZ demonstrating the best overall sliding wear behavior. Abrasion tests indicated good adhesion and coating integrity, and thermal expansion tests indicated that the two coatings were thermally compatible with SR34 steel. Tribocorrosion testing also showed that the two coatings were more resistant to wear and electrochemical degradation when used together, with CSZ showing the most consistent overall behavior. Overall, both coatings improved SR34 performance, but CSZ showed the most consistent behavior in piston rings.

Keywords calcia-stabilized zirconia, piston ring, SR34 steel, surface coating, tribocorrosion, tribological performance, yttria-stabilized zirconia

1. Introduction

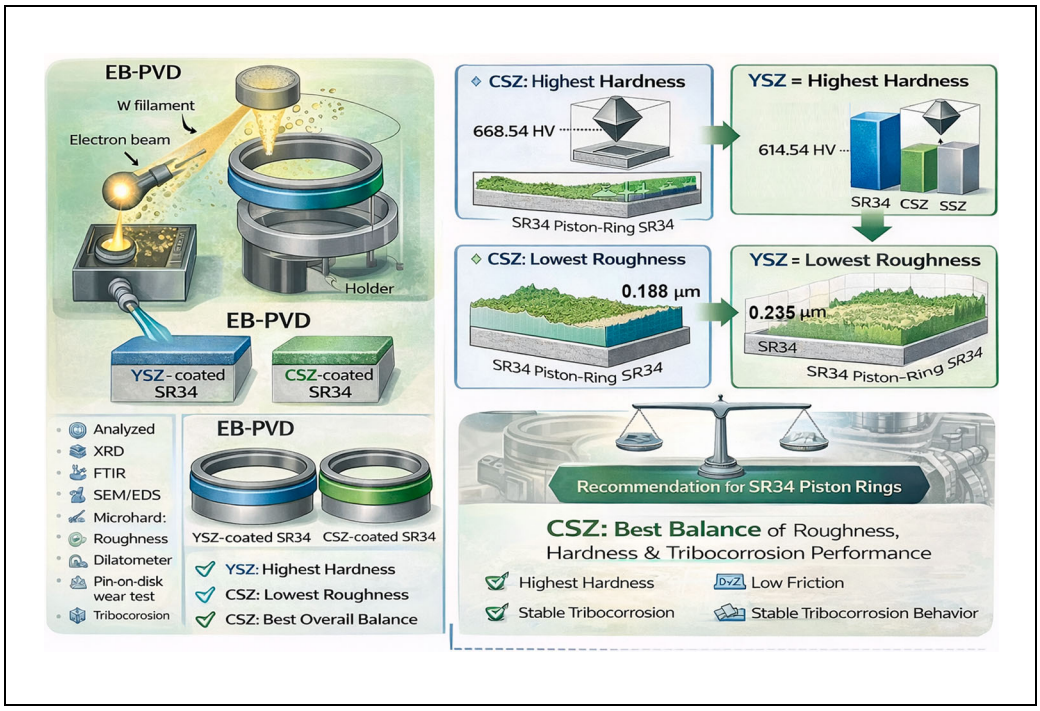
Enhancing the tribological performance of piston rings in internal combustion engines is also a significant step toward reducing frictional power loss, fuel consumption, and component degradation (Ref 1-3). The ring–liner contact is among the most highly loaded sliding interfaces within the piston assembly, as it must seal gases, retain oil, and withstand repeated reciprocating motion under mixed lubrication and high temperature (Ref 4-6). Past tribology research has shown that piston ring friction accounts for a significant portion of engine mechanical losses, and the top compression ring is especially problematic because it is closest to the combustion chamber and thus faces the greatest thermal and mechanical loads. (Ref 7-9). These service conditions predispose the top piston ring to wear due to friction, surface fatigue, and thermal damage, which can reduce service life and engine reliability (Ref 10, 11). The SR34 steel is an appropriate material for this application because it is a martensitic stainless steel developed for tight piston ring applications, as a combination of hardness, strength, wear resistance, and heat tolerance is required (Ref 12). In the current research, the chosen SR34 material had a hardness of 38-44 HRC, a tensile strength of approximately 1200 N/mm^2, and a coefficient of thermal expansion of 1.01×10^{-5} °C^{-1}, consistent with its use as a top piston ring material under extreme tribological conditions (Ref 13, 14). More generally, martensitic stainless steels are commonly used where high hardness and intermediate corrosion resistance are required (Ref 15).

In contrast, steel piston rings are typically made of chromium-containing martensitic alloys because they are compatible with surface engineering (Ref 16). However, bare

Uthirapathy Chandrasekaran, Department of Mechanical Engineering, SRM Institute of Science and Technology, Ramapuram, Chennai, Tamil Nadu 600089, India; **K. Hariharan**, Department of Mechanical Engineering, Dr Mahalingam College of Engineering and Technology, Pollachi, Tamil Nadu 642003, India; **Saravanan Raju**, Department of Mechanical Engineering, PSG Institute of Technology and Applied Research, Coimbatore, Tamil Nadu 641062, India; and **C. Ilamvazhuthi**, Department of Mechanical Engineering, EGS Pillay Engineering College (Autonomous), Nagapattinam, Tamil Nadu 611002, India. Contact e-mail: vijaymech51@gmail.com.

Published online: 16 October 2026

Graphical Abstract



steel surfaces are susceptible to abrasive and adhesive wear, frictional heating, and progressive roughening during operation, particularly when lubrication is locally depleted or the contact repeatedly heats up (Ref 17, 18). For these reasons, surface coating has emerged as an effective engineering approach to improving piston rings. A properly designed coating can enhance hardness, reduce direct metal-to-metal contact, improve wear resistance, stabilize friction, and provide thermal protection without affecting the bulk toughness of the substrate (Ref 19, 20). Electron beam physical vapor deposition (EB-PVD) is also a popular deposition technology, as it can form thin, uniform ceramic layers with excellent adhesion and typical strain-resistant microstructures (Ref 21, 22). EB-PVD zirconia coatings are known for their fine columnar structure, high-temperature stability, and resistance to thermal shock and cyclic loading, making them well suited for components subjected to repeated heating and sliding contact (Ref 23, 24). Therefore, adding an EB-PVD ceramic coating to SR34 steels is a promising way to extend the lifespan of top piston rings in harsh engine environments. Besides EB-PVD, electrodischarge coating (EDC) and electrospark deposition have emerged as effective surface modification techniques for improving the mechanical and tribological performance of engineering alloys (Ref 25, 26). Recent studies have demonstrated that EDC-based coatings using composite and powder metallurgy electrodes can enhance surface integrity, microhardness, wear resistance, and tribological behavior of metallic substrates (Ref 27, 28). However, EB-PVD zirconia coatings offer advantages in terms of ceramic layer uniformity, thermal stability, and high-temperature performance, making them suitable for demanding applications such as piston rings (Ref 29).

Among oxide ceramics are yttria-stabilized zirconia (YSZ) and calcia-stabilized zirconia (CSZ), both based on zirconia, whose phase stability and performance can be significantly enhanced by appropriate dopants (Ref 30, 31). Pure zirconia undergoes phase changes that can cause volume changes and may promote cracking during thermal cycling (Ref 32). Adding yttria or calcia can eliminate this instability and maintain the more useful tetragonal and/or cubic structures (Ref 33). Low thermal conductivity, high melting point, phase stability, and good thermal shock resistance are the most common attributes of YSZ that make it a standard ceramic coating material (Ref 34). CSZ is also appealing because calcium stabilization enhances zirconia's thermal and mechanical strength, and previous tribological experiments on CSZ surfaces have shown favorable wear behavior during sliding (Ref 23). This research aimed to coat YSZ and CSZ on SR34 steel using EB-PVD and systematically compare the two for top piston ring applications. The research focused on coating formation, microstructure, surface roughness, microhardness, sliding wear behavior, abrasion response, thermal expansion compatibility, and tribocorrosion. This research will help explain the effects of stabilized zirconia coatings on the functional surface of piston ring steel and identify a coating system that offers an optimum balance between tribological and thermal performance in advanced engine service. In the recent literature concerning this work, the system of the piston rings and the cylinder liner is of interest, with emphasis on the losses of friction, on the surface engineering, sensitivity to the working conditions and to zirconia-based coating, in particular, YSZ and, to a lesser degree, CSZ, with consideration of deposition route, phase stability, microstructure, hardness, wear, and thermal durability (Table 1).

Although surface coatings for piston rings are widely used, literature on ceramic coatings for zirconia-based piston ring steels remains limited. Most research on piston ring coatings has focused on nitrides, DLC, and Cr-based systems, with

Table 1 Literature summary of recent research on coating in the piston ring and materials

No.	Exact study	System/focus	Main findings relevant to this research	Relevance/limitation for the present work
1	Liu et al. (2025), (Ref 35)	Ring–liner friction pair morphology under different temperatures and loads	Shows that temperature and load strongly alter the microscopic wear morphology of piston ring–cylinder liner pairs.	Reinforces the need for surface engineering under severe service, but does not investigate ceramic zirconia coatings.
2	Wang et al. (2026), (Ref 36)	Piston ring–cylinder liner tribology under altered lubrication chemistry	Shows the PRCL pair is highly condition-sensitive; ammonia changed lubricant behavior and caused corrosive wear at room temperature. It also notes that the ring–liner pair contributes about 30–35% of the engine's mechanical losses.	Very recent engine tribology evidence, but not a coating development study.
3	Buitkenov et al. (2025), (Ref 37)	YSZ/NiCrAlY multilayer coating performance	Investigates the structure, phase composition, thermal corrosion, and tribological performance of YSZ-based multilayer coatings at high temperature.	Strongly supports YSZ relevance, but the substrate/system is TBC-oriented rather than piston ring steel.
4	Huo et al. (2025), (Ref 38)	EB-PVD YSZ process optimization	Shows oxygen gas flow strongly affects the surface and cross-sectional microstructure of EB-PVD YSZ; insufficient oxygen can create an interlayer defect and reduce thermal shock life.	Highly relevant to EB-PVD YSZ processing, but centered on TBC lifetime rather than tribology on SR34.
5	Banerjee et al. (2023), (Ref 39)	Wear-based evaluation of YSZ coating durability	Links wear resistance, profilometry, specific wear rate, and COF to YSZ service life, and identifies optimized yttrium content.	Important for tribological evaluation methodology, but not specific to piston ring substrate/coating pairing.
6	Gao et al. (2021), (Ref 40)	YSZ on stainless steel under tribo-corrosion	The YSZ coating shows much lower corrosion current density and lower wear/corrosion volume loss than bare stainless steel.	Supports the protective role of YSZ on steel substrates, but the environment and application conditions differ from those of engine piston rings.
7	Küçük (2020), (Ref 41)	CSZ coating tribology	Demonstrates that counterbody selection significantly influences the dry sliding wear of CSZ coatings.	Especially relevant because CSZ-specific tribology literature is limited; however, the coating was plasma-sprayed and not applied to SR34 piston ring steel.
8	Loghman-Estarki et al. (2016), (Ref 42)	Nanostructured ScYSZ and YSZ top coats with NiCrAlY bond coat deposited on IN738LC by APS;	ScYSZ exhibited better hot-corrosion resistance than YSZ.	It supports the importance of zirconia-based coatings for high-temperature applications.
9	Lin et al. (2016), (Ref 43)	TiSiCN nanocomposite coatings deposited by plasma-enhanced magnetron sputtering (PEMS) on stainless steel.	The optimized TiSiCN coating showed excellent adhesion, low dry COF, and improved piston ring performance. In engine tests, coated rings reduced piston assembly friction contribution and showed 29% lower top ring weight loss and 40% lower second ring weight loss than the uncoated rings.	This paper strongly underscores the importance of surface coatings for reducing friction and wear in piston rings and justifies tribological testing under real engine contact conditions.
10	Keyvani et al. (2017), (Ref 44)	YSZ and CSZ coatings	The study found that CSZ had smaller, more uniform pores and exhibited better sintering behavior, lower thermal stress, and superior thermomechanical performance than YSZ during thermal cycling.	This is the most directly relevant of the three uploaded papers because it compares YSZ and CSZ and discusses microstructure, hardness, elastic modulus, and thermal expansion, which closely aligns with your comparison of YSZ- and CSZ-coated SR34 steel.

zirconia coatings primarily explored for thermal barrier or corrosion protection applications. Moreover, zirconia research primarily focuses on YSZ, and comparative studies on CSZ remain limited, particularly under the tribological conditions of engine components. Currently reported coating studies on zirconia also tend to use superalloys or ordinary stainless steels rather than SR34 martensitic piston ring steel, making it hard to assess coating–substrate interactions and performance directly in actual piston ring service. Another major weakness in the literature is that most studies focus on a single property (e.g., phase stability, hardness, wear, or thermal behavior) rather than providing a comprehensive assessment of coating performance. Specifically, the literature does not address the combined effects of coating chemistry, microstructure, roughness, hardness, lubricated sliding wear on cast iron, abrasion resistance, thermal compatibility, and tribocorrosion behavior of both YSZ and CSZ on the same substrate (piston ring).

This gap is addressed by the current study, which provides a direct, side-by-side comparison of EB-PVD YSZ and EB-PVD CSZ coatings on SR34 steel as top piston ring coatings. Unlike most of the available literature, which is coating process-based or focuses on a single or two properties, this study relates processing, structure, surface condition, tribological response, thermomechanical compatibility, and tribocorrosion resistance within a single application-driven framework. The study's originality lies in three aspects. First, it uses SR34 steel, a convenient piston ring substrate rather than a generic laboratory alloy. Second, it contrasts two stabilized zirconia systems under the same deposition route and test conditions, providing a clear basis for coating selection. Third, it extends beyond traditional coating characterization by incorporating tribocorrosion to better reflect what actually happens to piston rings in service, in a combined mechanical and chemical environment. Consequently, the research not only presents novel comparative data but also offers a viable engineering recommendation: YSZ is the most suitable for hardness, whereas CSZ is the most balanced overall for SR34 top piston ring applications.

2. Materials and Methods

2.1 Materials

This work investigated three groups of specimens: uncoated SR34 steel, YSZ-coated SR34 steel, and CSZ-coated SR34 steel. SR34 was adopted as the sample material in Fig. 1, since the top piston ring undergoes extreme thermomechanical and tribological conditions, and the piston ring–liner interface is considered one of the most important friction and wear interfaces in internal combustion engines.

Moreover, SR34 is a popular 18% Cr martensitic stainless steel used in piston rings, making it a suitable 18% Cr martensitic industrial substrate for testing advanced ceramic surface modifications. YSZ and CSZ are chosen as ceramic coating materials because they offer a good balance of high hardness, relatively low thermal conductivity, chemical stability, and resistance to thermal degradation. Pure zirconia undergoes monoclinic, tetragonal, and cubic phase transitions as a function of temperature; as the material cools, these transformations can cause volume changes, residual stresses, and cracking. This instability is suppressed by yttria or calcia, which stabilize the more thermally stable tetragonal and/or cubic phases, which is why these materials are commonly used in protective ceramic coatings (Ref 45, 46). Table 2 summarizes the nominal chemical composition and baseline engineering properties of the SR34 substrate used in this study. Table 3 lists the nominal physical properties of the YSZ and CSZ feed materials used to be deposited.

2.2 EB-PVD coating deposition

YSZ and CSZ coatings were also deposited on SR34 substrates with the help of an electron beam physical vapor deposition system. EB-PVD was chosen because it forms smooth, dense-to-columnar ceramic coatings with good adhesion and high strain capacity. In zirconia-based systems, EB-PVD coating is particularly appreciated for its typical columnar morphology and relatively smooth surface, both of which are beneficial under thermal and tribological loading (Ref 47).

In the current test, the SR34 samples were mounted on a rotating substrate holder driven by an AC geared motor. A rotary vacuum pump, a rotary roots pump, a diffusion pump, and a holding pump evacuated the coating chamber. Microprocessor-controlled Pirani–Penning gauges monitored chamber pressure. Before deposition, the mounted specimens were ion-cleaned in a controlled argon environment using an ion bombardment target to remove remaining rust, oil, and surface contaminants and enhance coating adhesion. A dome-shaped heater heated the substrates, and a digital PID controller and K-type thermocouple regulated the temperature. Once thermally stabilized, a water-cooled, magnetically focused, bent-beam electron gun evaporated the ceramic feed material, and the vapor flux condensed on the rotating SR34 substrates to form the ceramic coating layer. Table 4 lists the nominal deposition conditions for this study. Figure 2 shows the coating process and coated samples.

2.3 Surface and microstructural characterization

Scanning electron microscopy (SEM) was used to characterize the surface morphology and microstructural features of the uncoated and coated specimens. After tribological testing, SEM assessed coating continuity, surface topography, particle characteristics, porosity, microcracks, droplets, and wear track morphology. For coated specimens, cross-sectional analysis evaluated coating thickness uniformity, interfacial integrity, and the potential for local delamination or decohesion at the coating/substrate interface. The elemental composition of the deposited layers was also determined using energy-dispersive X-ray spectroscopy (EDS) (Ref 48). Compositional evidence of successful deposition of the desired stabilized zirconia and Ca in CSZ-coated specimens served as evidence of the detectable presence of Zr and O, along with Y in YSZ-coated specimens.

2.4 Surface roughness measurement

A non-contact optical profilometry system (Mirau interferometry) with a 20x objective was used to measure surface topography and roughness. Minimize local bias, take roughness measurements at several random points on each sample, and report the results as the mean and standard deviation (Ref 49). This is particularly relevant to the current work, as coating-induced changes in asperity structure may directly affect friction, running-in behavior, and the wear response of piston ring materials.

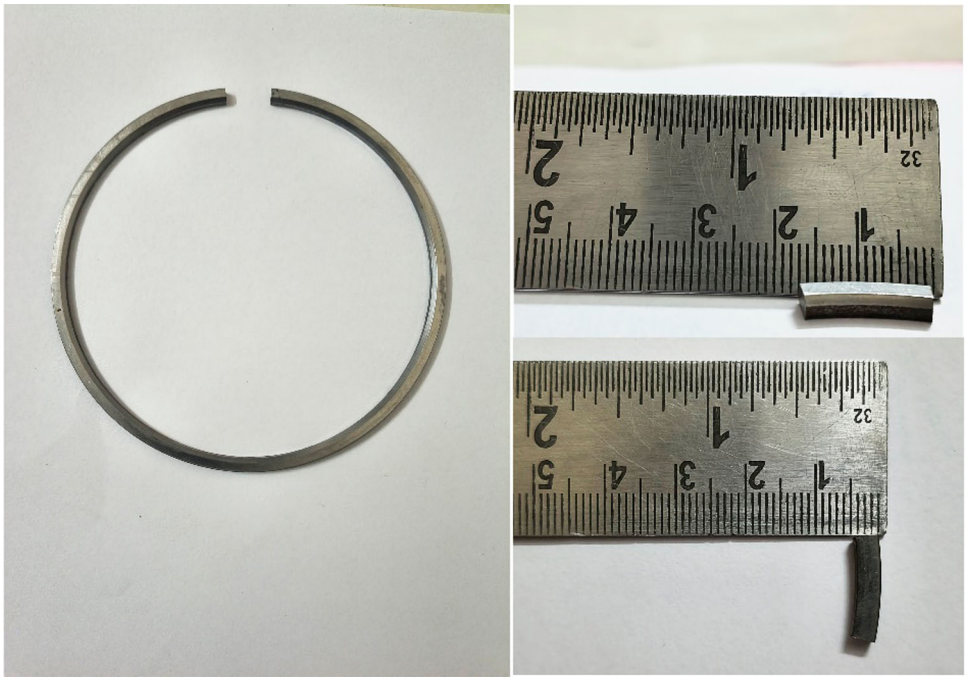


Fig. 1 SR34 piston ring used in the study

Table 2 Nominal composition and baseline properties of the SR34 substrate used in this study

Parameter	Value
C, wt.%	0.80-0.95
Si, wt.%	0.35-0.50
Mn, wt.%	0.25-0.40
P, wt.%	≤ 0.040
S, wt.%	≤ 0.040
Cr, wt.%	17.0-18.5
Mo, wt.%	1.00-1.25
V, wt.%	0.08-0.15
Hardness	38-44 HRC
Tensile strength	~ 1200 N/mm^2
Young's modulus	200,000 N/mm^2
Coefficient of thermal expansion (20-300 °C)	1.01 × 10^{-5} °C^{-1}

Table 3 Nominal properties of YSZ and CSZ coating feed materials

Property	YSZ	CSZ
Density	6.00 g/cm^3	6.10 g/cm^3
Compressive strength	2600 MPa	2800 MPa
Flexural strength	900 MPa	950 MPa
Thermal conductivity	2.0 W/m·C	2.2 W/m·C
Coefficient of thermal expansion	11.4 × 10^{-6}/°C	12.5 × 10^{-6}/°C

2.5 Microhardness measurement

Vickers hardness testing was used to evaluate the indentation response of the uncoated and coated SR34 specimens. The Vickers hardness method uses a diamond indenter in the form of a square-based pyramid with a 136° angle between opposite faces. During the test, the indenter is pressed into the specimen surface under a controlled test force and held for a dwell time of approximately 10–15 s. After removal of the load, the two diagonals of the square-shaped indentation are measured optically, and their average value is used to calculate the Vickers hardness number (Ref 50). The Vickers hardness value is calculated using Eq 1:

$$HV = \text{Constant} \times \text{test force}/\text{indent diagonal}^2 \quad \text{(Eq 1)}$$

Table 4 EB-PVD system characteristics and deposition conditions used for YSZ and CSZ coatings

Parameter	Value
Substrate material	SR34 stainless steel
Coating materials	YSZ and CSZ
Ultimate chamber vacuum	5 × 10^{-7} mbar
Working/deposition pressure	5 × 10^{-6} mbar
Substrate holder speed range	2–30 rpm
Substrate rotation during deposition	15 rpm
Substrate temperature	250 °C
Maximum heater temperature	350 °C
Ion cleaning source	Ar ion bombardment
Ion bombardment power	3.5 kV, 500 mA max
EB-gun pressure capability	below 5 × 10^{-4} mbar
EB-gun power rating	6–8 kW during deposition
Beam voltage	4–10 kV DC
Beam current	0–1 A
Filament current	0–20 A during deposition
Filament voltage	0–10 V AC
Beam deflection	270°
Beam spot size	~ 6 mm × 10 mm
Evaporation rate	0–2 Å/s
Nominal coating thickness	~ 1 μm

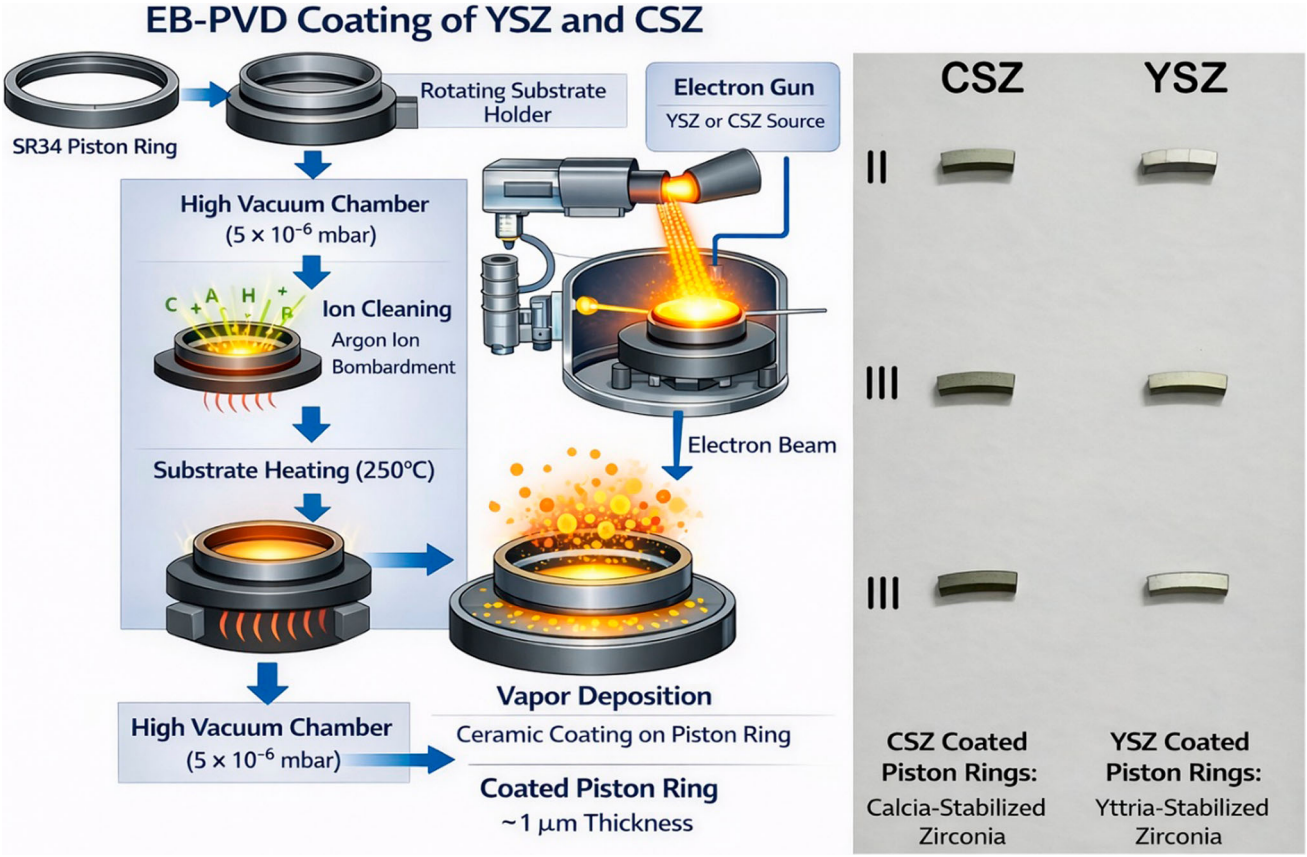


Fig. 2 Illustration of the coating process and coated samples

where the constant depends on the indenter geometry and the units used for force and indentation diagonal. In standard Vickers testing, ASTM E384 covers the micro-force range, typically from 10 gf to 1 kgf, whereas ASTM E92 covers the macro-force range from 1 to 100 kgf. ISO 6507-1, ISO 6507-2, and ISO 6507-3 also define the Vickers hardness method for micro- and macro-hardness testing.

In the present study, the measured hardness values of the coated specimens were interpreted as apparent composite surface hardness values of the coating/substrate system rather than the intrinsic hardness of the ceramic coating. This consideration is important because the EB-PVD YSZ and CSZ coatings were approximately 1 μm thick. During Vickers indentation, the plastic deformation zone extends beneath the indentation impression and may exceed the coating thickness, resulting in interaction between the ceramic layer and the SR34 substrate. Therefore, the measured hardness response represents a combined contribution from the hard zirconia coating and the comparatively softer steel substrate. To accurately determine coating-only hardness, techniques such as nanoindentation with controlled penetration depth are required. Therefore, the reported hardness values should not be considered the intrinsic hardness of the isolated ceramic coating layer. At least five indentations were made at different locations on each specimen, and the mean value and standard deviation were reported. For accurate determination of coating-only hardness in future work, nanoindentation or very low-load indentation with controlled penetration depth would be required.

2.6 Sliding Wear Test

A pin-on-disk tribometer was used to evaluate the lubricated sliding wear behavior of uncoated SR34, YSZ-coated SR34, and CSZ-coated SR34 specimens against a cast iron counter-face. The test followed ASTM G99, a standard commonly used for laboratory wear and friction testing with pin-on-disk or ball-on-disk configurations. In the present study, each specimen group was tested under two loading conditions, 5 and 10 kg, corresponding to approximate normal forces of 49.05 and 98.10 N, respectively. The rotational speed was maintained at 900 rpm, and the test duration was 900 s for each condition. During sliding, the coefficient of friction was recorded continuously. The mass loss measured before and after sliding was converted to wear volume using the density of the corresponding material. The wear volume was calculated as: (Ref 51, 52)

$$V = \Delta m/\rho \qquad \text{(Eq 2)}$$

where V is the wear volume, Δm is the mass loss, and ρ is the density. Since Δm was measured in grams and density was expressed in g/cm^3, the calculated volume was converted to mm^3 by multiplying by 1000. The densities used for wear volume calculation were 7.75 g/cm^3 for uncoated SR34 steel, 6.00 g/cm^3 for YSZ, and 6.10 g/cm^3 for CSZ. For the coated specimens, the corresponding coating density was used because the wear track was mainly confined to the coating layer. The specific wear rate was then calculated using k = V/WS, where k is the wear rate in mm^3/Nm, W is the normal load in N, and S is the total sliding distance in m.

2.7 Microabrasion behavior and coating thickness measurement

A ball-cratering microabrasion test measured the abrasion level. For this technique, a rotating HCHCR steel ball (25 mm in diameter) was brought into contact with the coated surface in the presence of a diamond suspension, thereby forming a wear crater via progressive microabrasion. In this study, the test was conducted at a load of 20N, a rotational speed of 300 rpm, and a test time of 20 min. The crater geometry was optically measured after abrasion, and the coating thickness was estimated from it. In terms of D and d, the outer and inner crater diameters, respectively, the coating thickness is expressed as Eq 3 (Ref 53):

$$t = \frac{D^2 - d^2}{8R} \quad \text{(Eq 3)}$$

where t is the coating thickness and R is the radius of the ball.

2.8 Thermal Expansion Analysis

The dilatometry behavior of the uncovered and coated specimens at 1000 °C was measured with a push-rod dilatometer. The test follows ASTM E228, which establishes the linear thermal expansion of rigid solid materials using push-rod dilatometers. The coefficient of thermal expansion is obtained from Eq 4:

$$\alpha = \frac{\Delta L}{L_0 \Delta T} \quad \text{(Eq 4)}$$

where α is the linear coefficient of thermal expansion, ΔL is the measured change in length, L_0 is the original specimen length, and ΔT is the applied temperature interval.

2.9 Tribocorrosion Testing

The tribocorrosion behavior of uncoated SR34, YSZ-coated SR34, and CSZ-coated SR34 was tested in a tribometer-based three-electrode electrochemical cell in the presence of 3.5 wt.% NaCl at 25 °C under naturally aerated conditions. Flat SR34 coupons that had been coated with the same EB-PVD batch as the piston ring specimens in the EB-PVD batch were epoxy-mounted, with the remaining 1.0 cm^2 as the working area (Ref 54). A cast iron counterbody ensured relevant piston ring contact conditions. The normal force was 5 N, the sliding velocity was 0.05 m/s, the radius of the wear track was 5 mm, and the period of sliding was 1800 s (Ref 55). The specimens were equilibrated at open-circuit potential for 60 min and then allowed to slide, with simultaneous electrochemical and friction monitoring during sliding and a 30-min post-sliding recovery period. Polarization resistance measurements were conducted in the range ± 10 mV around OCP, and EIS was performed at OCP from 100 kHz to 10 mHz with a perturbation of 10 mV (Ref 56). The 3.5 wt.% NaCl solution at 25 °C was used as a controlled laboratory electrolyte to compare the relative tribocorrosion resistance of uncoated SR34, YSZ-coated SR34, and CSZ-coated SR34 under identical electrochemical and sliding conditions. This environment does not fully reproduce piston ring service conditions, where the surface is exposed to engine oil, elevated temperature, lubricant degradation products, moisture, and combustion by-products. Therefore, interpret the present tribocorrosion results as laboratory-scale comparative screening data rather than direct engine service performance. Future work should include high-temperature reciprocating tests in engine oil or simulated combustion-contaminated lubricant environments.

2.9.1 Test Repetitions and Statistical Analysis. For all experimental investigations, the number of specimens, measurement locations, and test repetitions were specified to ensure repeatable, reliable results. Three specimens were used for each sample group, namely uncoated SR34, YSZ-coated SR34, and CSZ-coated SR34, wherever applicable. Surface roughness was measured at five locations on each specimen. Apparent Vickers hardness was measured using five indentations at different locations on each specimen. Sliding wear tests were repeated three times for each sample group at both 5 kg and 10 kg loads. Micro-abrasion and coating thickness measurements were performed on three coated specimens for each coating type. Thermal expansion testing was conducted using three specimens for each sample group. Tribocorrosion tests were also repeated three times for each sample group under identical test conditions. Quantitative results were expressed as mean ± standard deviation wherever repeated measurements were available. Representative curves were presented for the coefficient of friction, OCP, polarization, and EIS responses, while the corresponding numerical values were used for comparative analysis.

3. Results and Discussion

3.1 FTIR Analysis of Uncoated SR34, YSZ-Coated, and CSZ-Coated Samples

Figure 3 shows the FTIR spectra of the uncoated SR34 substrate and the SR34 specimens coated with YSZ and CSZ in the spectral range of 400-4000 cm^{-1}, and the representative FTIR peak assignments are listed in Table 5. A general feature of all spectra will be a broad absorption band in the 3000-3500 cm^{-1} region, along with a weaker band at 1630-1640 cm^{-1}. These bands are normally attributed to the stretching vibration of surface hydroxyl groups and the bending

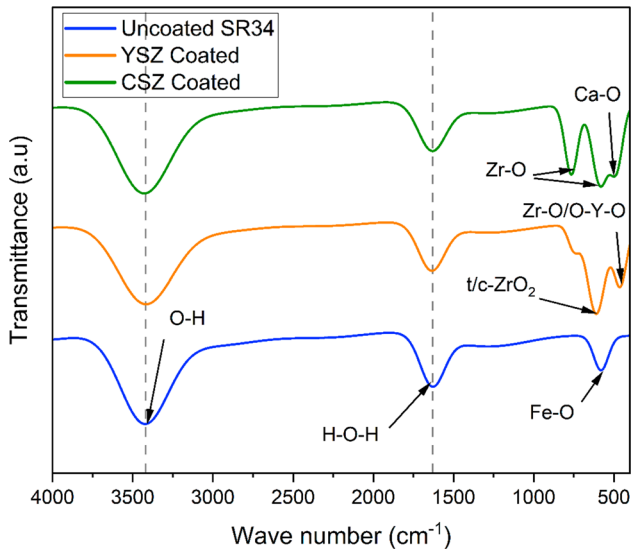


Fig. 3 Representative FTIR spectra of uncoated SR34, YSZ-coated SR34, and CSZ-coated SR34

Table 5 Representative FTIR peak assignments for uncoated SR34, YSZ-coated SR34, and CSZ-coated SR34 samples

Sample	Wavenumber (cm^{-1})	Assignment	Interpretation
Uncoated SR34	3430-3450	O–H stretching	Surface hydroxyl groups / adsorbed moisture
Uncoated SR34	1630-1640	H–O–H bending	Molecular water adsorbed on passive oxide film
Uncoated SR34	570-600	Fe–O / oxide-related vibration	Native/passive iron-rich surface oxide contribution
YSZ-coated SR34	3420-3450	O–H stretching	Hydroxylated ceramic surface / adsorbed moisture
YSZ-coated SR34	1630-1640	H–O–H bending	Adsorbed water on the oxide coating surface
YSZ-coated SR34	600-610	Zr–O vibration, tetragonal/cubic zirconia related	Evidence of stabilized zirconia lattice
YSZ-coated SR34	450-460	Zr–O / O–Y–O or Zr(Y)–O vibration	Confirms Y-containing stabilized zirconia environment
YSZ-coated SR34	~ 755 (weak/optional)	Monoclinic zirconia-related band	Weak intensity suggests limited monoclinic content
CSZ-coated SR34	3430-3450	O–H stretching	Hydroxylated ceramic surface/adsorbed moisture
CSZ-coated SR34	1630-1640	H–O–H bending	Adsorbed water
CSZ-coated SR34	~ 482	Ca–O vibration	Evidence of calcia incorporation
CSZ-coated SR34	~ 585	Zr–O vibration	Stabilized zirconia framework
CSZ-coated SR34	~ 765	Zr–O vibration	Further confirmation of CSZ formation

vibration of physisorbed molecular water on the adsorbed surface, respectively, indicating the presence of surface hydroxylation and physisorbed moisture on oxide-containing surfaces (Ref 57).

The bare SR34 substrate has a relatively featureless spectrum with weak hydroxyl/water-related absorptions and a low-intensity band in the iron-oxide region (570 to 600 cm^{-1}). This profile is consistent with the passive oxide/hydroxide film typically present on steel surfaces exposed to the atmosphere. The relatively low intensity of this low-wavenumber band in the coated samples suggests that the substrate spectrum is dominated by the metallic base, with surface oxide species contributing only a small amount. Therefore, the uncoated sample serves as a good control for evaluating the chemical alterations induced by the zirconia coatings.

Following EB-PVD deposition of YSZ, the FTIR spectrum should show a significant change in absorption strength in the zirconia lattice region. Specifically, bands around 600-610 cm^{-1} and 450-460 cm^{-1} correspond to Zr-O-related lattice vibrations and O–Y–O/Zr(Y)–O bonding conditions in yttria-stabilized zirconia. The 600 cm^{-1} band is commonly assigned to tetragonal zirconia in zirconia systems, and a typical Zr-O band appears at 460 cm^{-1}. The emergence and intensification of these features relative to the substrate affirm the successful development of a YSZ coating on SR34. The CSZ-coated sample will show a similar hydroxyl/water envelope at high wavenumbers, with a different low-wavenumber fingerprint due to both zirconia and calcium bonding. According to the reported FTIR behavior of CSZ, bands around ~ 482 cm^{-1} are attributed to Ca-O vibrations, and peaks around 585 cm^{-1} and 765 cm^{-1} are attributed to Zr-O vibrations in the stabilized zirconia network. The simultaneous presence of these three bands provides strong spectroscopic evidence for the successful integration of calcium into the zirconia structure and the formation of a CSZ coating. The CSZ spectrum can thus exhibit a more complex band structure in the 450-800 cm^{-1} region due to an additional Ca-O contribution, compared to YSZ.

Overall, the FTIR results support the successful deposition of zirconia-based ceramic coatings on SR34 steel. The very weak, comparatively simple spectrum of the uncoated substrate contrasts with the high-strength, more structured low-wavenumber response of the coated specimens. A sample that is YSZ-coated is characterized by the prominent zirconia lattice bands around the vicinities of ~ 610 and 460 cm^{-1}. In contrast, a sample that is CSZ-coated is characterized by the additional CaO-related band around the vicinities of 482 cm^{-1}, along with the ZrO bands around 585 and 765 cm^{-1}. In terms of material performance, these observations are significant because they confirm the presence of chemically stable oxide ceramic layers, which are predicted to enhance the hardness, wear resistance, and thermal stability of the top piston ring surface.

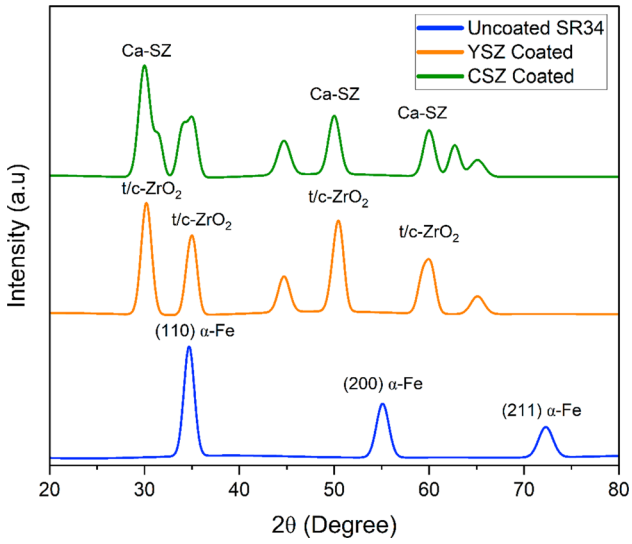


Fig. 4 Representative XRD patterns of uncoated SR34, YSZ-coated SR34, and CSZ-coated SR34 samples, showing substrate-related reflections and zirconia-related diffraction features in the coated specimens

3.2 XRD Analysis of Uncoated SR34, YSZ-Coated, and CSZ-Coated Samples

Figure 4 shows the typical XRD patterns of the uncoated SR34 substrate and SR34 samples coated with YSZ and CSZ. The uncoated substrate diffractogram is dominated by the typical ferrite/martensite reflections of the steel matrix. The primary body-centered cubic α-Fe/martensite reflections are typically observed at 2θ = 34.7° (110), 55.1° (200), and 72.3°

(211) in martensitic or ferritic–martensitic steels. In similar martensitic stainless steels, XRD patterns have also been reported to show only ferrite/martensite characteristic peaks, with retained austenite either absent or below the practical detection limit.

The emergence of new diffraction peaks in the low-angle region after EB-PVD of YSZ confirms the growth of a crystalline zirconia ceramic layer on the SR34 substrate. The strongest reflections expected in YSZ occur at about $2\theta = 30.2°$, 35.2°, 45.2°, 50.2°, 60.2°, and 62.2°, and these are generally cited as typical of tetragonal zirconia. The sharp peak at about 30.2° and the reflections at about 35.2°, 50.2°, and 60.2° are of particular interest because they indicate that zirconia has stabilized and is no longer in the monoclinic room-temperature form but rather in the tetragonal/t-type form, which is typically associated with greater mechanical reliability. An important consideration when interpreting YSZ diffraction patterns is that the tetragonal and cubic zirconia structures can be difficult to distinguish with standard XRD because their lattice parameters are very close and certain reflections overlap to the point of coinciding. Separating t, t, and c contributions often requires high-resolution analysis or Rietveld refinement to be confident.

The CSZ-coated sample also displays a crystalline pattern based on zirconia, with peak positions and relative intensities similar to those of calcia-stabilized zirconia. The most commonly reported XRD patterns of calcia-stabilized zirconia exhibit major reflections at $2\theta = 30°$, 31.5°, 34°, 45°, 50°, and 60.7°, characteristic of stabilized tetragonal and/or cubic zirconia. Studies on partially stabilized zirconia also report that the highest zirconia peaks are cubic and tetragonal, with 2θ usually at 50° and 60°. The presence of these reflections in the coated sample consequently supports the effective development of a CSZ layer on the SR34 surface.

Overall, the XRD results confirm successful deposition of crystalline stabilized zirconia coatings on SR34 steel. The uncoated sample exhibited characteristic ferrite/martensite substrate reflections, whereas the YSZ- and CSZ-coated samples showed additional zirconia-related diffraction peaks in the 30–63° range. The YSZ coating exhibited reflections corresponding to stabilized tetragonal zirconia, while the CSZ coating showed diffraction features associated with calcium-stabilized zirconia containing tetragonal/cubic zirconia components. However, accurately distinguishing between tetragonal and cubic zirconia phases is challenging because their lattice parameters are closely related and their diffraction peaks overlap, particularly in thin coatings. In this study, XRD analysis was limited to qualitative phase identification, and we did not perform quantitative phase determination. Advanced analysis methods such as Rietveld refinement, high-resolution XRD, and PDF database matching would be required to quantify the relative tetragonal and cubic phase fractions. Therefore, the current XRD results confirm zirconia-based coating formation rather than providing quantitative phase analysis.

3.3 SEM/EDS Analysis

3.3.1 CSZ-coated SR34 Steel. Figure 5 confirms the successful deposition of a continuous CSZ coating on an SR34 steel substrate, as shown by the cross-sectional SEM micrographs. The coating thickness was measured at multiple locations from the cross-sectional SEM micrographs to evaluate deposition uniformity. The average CSZ coating thickness was 1.16 ± 0.06 μm. The low standard deviation confirms uniform deposition and indicates good control of the EB-PVD coating process. The interface between the coating and substrate is well defined and in phase, with no apparent through-thickness cracks, gross pores, or interfacial delamination visible in the studied area. The undulated interface can also promote mechanical interlocking between the ceramic layer and the substrate, albeit to a slight extent. At higher magnification, the coating shows a fine, compact morphology, which is more suitable for a thin tribological coating used in piston ring applications.

The EDS point spectrum also supports the formation of a calcium-stabilized zirconia layer. The detected elements were C (34.20 wt.%), O (48.85 wt.%), Ca (4.28 wt.%), Fe (10.00 wt.%), and Zr (2.66 wt.%). The relatively high carbon content detected in the EDS spectrum is attributed to possible contamination introduced during metallographic preparation, including mounting materials, polishing media, or surface adsorption during handling. Since carbon was not present in the CSZ feed material, it is not considered to be a constituent of the deposited coating. Furthermore, because the CSZ coating thickness is approximately 1 μm, the electron beam interaction volume may extend beyond the coating region and detect signals from surface residues and the underlying substrate. Therefore, the carbon peak is considered a preparation-related contribution, whereas the simultaneous detection of Ca, Zr, and O confirms the formation of the calcium-stabilized zirconia coating. The simultaneous detection of Ca, Zr, and O confirms the presence of the CSZ coating (Table 6). In contrast, the Fe signal arises from the substrate (SR34) because the coating is thin and the interaction volume is large at 15 kV. The elevated carbon content likely reflects sample preparation or surface contamination and should not be considered part of the coating. Although the absolute EDS values are semi-quantitative, the SEM/EDS data indicate that a thin, continuous, and adherent CSZ coating was deposited on SR34 steel and is likely to enhance the tribological life of the top piston ring.

3.3.2 YSZ-coated SR34 Steel. Figure 6 confirms the successful deposition of a continuous YSZ coating on the SR34 steel substrate, as shown in cross-sectional SEM micrographs. The YSZ coating thickness was determined from multiple measurements obtained from different regions of the cross-sectional SEM images. The average coating thickness was calculated as 1.35 ± 0.05 μm, indicating uniform deposition with limited thickness variation. The obtained thickness confirms successful formation of a continuous thin ceramic layer on the SR34 substrate. However, the coating remained within the thin-film range and formed a distinct, continuous layer over the substrate. The coating/substrate interface was clearly observed and appeared coherent, with no visible signs of significant delamination, spallation, or through-thickness cracking in the test area. The YSZ layer conformed to the substrate's local surface morphology and exhibited a fine, compact structure, characteristic of a thin EB-PVD ceramic gradient.

The EDS point spectrum from the coated region showed C (32.69 wt.%), O (24.44 wt.%), Fe (34.22 wt.%), Y (6.25 wt.%), and Zr (2.40 wt.%). The carbon signal in the YSZ-coated sample likely arises from external contamination rather than the deposited ceramic layer. During specimen

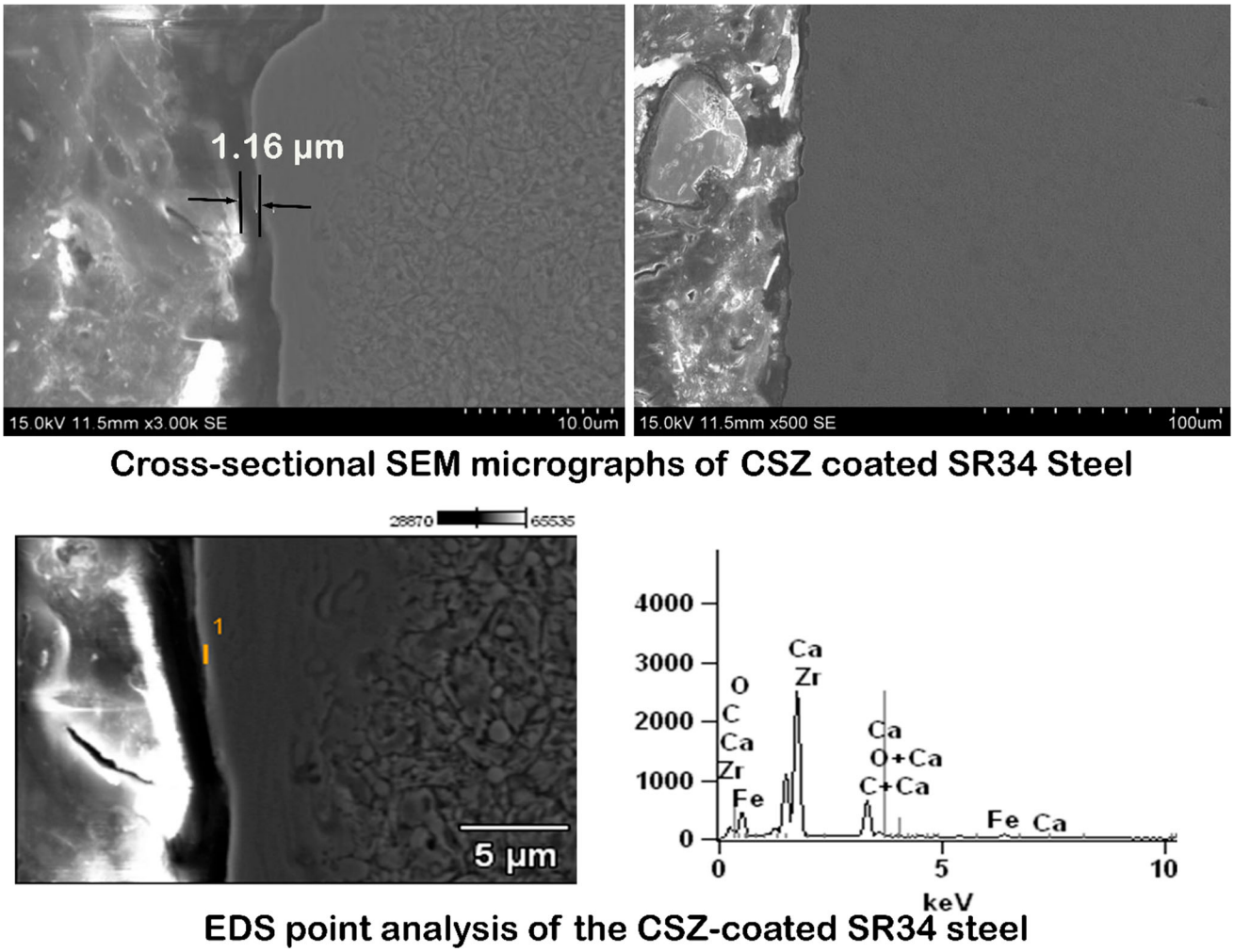


Fig. 5 Cross-sectional SEM micrographs and EDS point analysis of the CSZ-coated SR34 steel

Table 6 EDS point analysis of the CSZ-coated SR34 steel sample

Point ID	C, wt.%	O, wt.%	Ca, wt.%	Fe, wt.%	Zr, wt.%	Interpretation
CSZ-coated sample _pt1	34.20	48.85	4.28	10.00	2.66	Confirms local presence of calcia-stabilized zirconia coating; Fe arises from substrate contribution due to thin-film thickness.

preparation, carbon-containing residues from mounting, polishing, or environmental exposure may remain on the surface and contribute to the EDS response. Moreover, the thin EB-PVD coating allows the electron beam to partially interact with adjacent regions, which can influence the detected elemental composition. Therefore, carbon does not indicate carbon incorporation into the YSZ coating. The formation of the YSZ layer was confirmed by the characteristic presence of Y, Zr, and O signals, along with the continuous coating morphology observed in SEM. The simultaneous presence of Y, Zr, and O confirms the formation of a yttria-stabilized zirconia (YSZ) coating layer (Table 7). The comparatively high Fe concentration likely comes from the substrate, as the coating layer was thin (1.35 μm) and the analysis was conducted at 15 kV. The high carbon content likely results from sample preparation or surface contamination rather than the coating itself. Although the absolute EDS values are semi-quantitative, the SEM/EDS results confirm that we have deposited a thin, continuous, and adherent YSZ layer on SR34 steel, which should enhance the performance of the top piston ring on the surface.

3.4 Surface Roughness Analysis

The surface roughness results indicate a significant decrease in roughness following EB-PVD coating of SR34 steel stabilized with zirconia. The arithmetic average roughness (Ra) values were calculated from multiple measurements performed at different locations on each specimen and are presented as mean ± standard deviation. The uncoated SR34

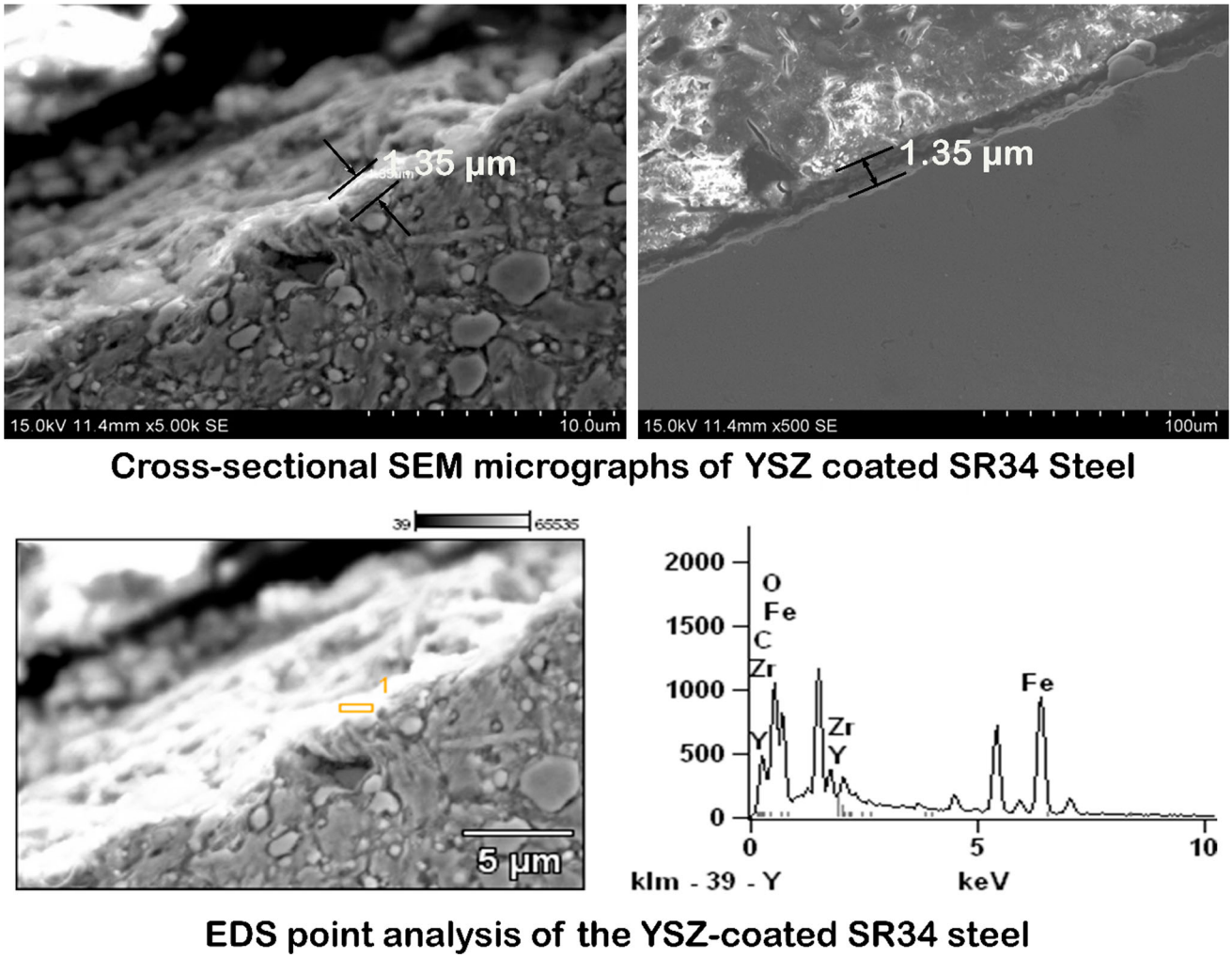


Fig. 6 Cross-sectional SEM micrographs and EDS point analysis of the YSZ-coated SR34 steel

substrate exhibited a Ra value of 0.274 ± 0.018 μm, whereas the YSZ- and CSZ-coated specimens showed values of 0.235 ± 0.015 and 0.188 ± 0.012 μm, respectively. The small standard deviations demonstrate good repeatability of the profilometry measurements and indicate uniform surface characteristics after coating deposition. This translates to a 14.23% reduction in Ra for YSZ versus the uncoated substrate and a 31.39% reduction in Ra for CSZ versus the uncoated substrate, with the CSZ surface being 20.0% smoother than the YSZ-coated surface. A similar trend is observed in Rq, which dropped to 0.286 μm for YSZ and 0.247 μm for CSZ, indicating that coating deposition suppresses height fluctuations. Table 8 supports this trend with the amplitude parameters.

The low standard deviation values associated with the measured roughness parameters indicate consistent surface characterization across the evaluated regions. Among the investigated samples, the CSZ-coated surface exhibited the lowest variation and roughness magnitude, confirming the formation of a relatively uniform and smooth ceramic coating surface. The bare SR34 substrate had the highest overall roughness, with Rz = 1.77 μm and Rt = 2.06 μm, indicating larger peak-to-valley variations across the measured profile (Fig. 7). After coating, the YSZ-coated surface had Rz = 1.54 μm and Rt = 1.75 μm, and the CSZ-coated surface had the lowest values, Rz = 1.47 μm and Rt = 1.68 μm. These results suggest that both coatings leveled the initial surface asperity field, but the CSZ coating had the greatest flattening effect. Practically, this implies that the coating process reduced the prominence of sharp summits and the vertical height distribution of the surface profile, which is desirable for minimizing localized contact stress during sliding.

The YSZ-coated specimen maintained a relatively high positive summit height (Rp = 0.829 μm). However, it reduced the maximum valley depth to Rv = 0.707 μm, indicating that the coating primarily softened deep depressions while retaining some summit structure. By contrast, the CSZ-coated sample exhibited the lowest peak height (Rp = 0.542 μm) among all the samples, indicating that it suppresses protruding asperities more effectively. Although its valley depth (Rv = 0.933 μm) was relatively high, the lower Ra, Rq, Rz, and Rt values suggest that the overriding influence of CSZ deposition was the flattening of surface peaks rather than the complete removal of all valleys (Ref 58). In tribological contacts, this positive effect can occur because a smoother summit can lead to less abrasive interaction and plowing, with some valley structure remaining under service conditions to allow debris accommodation or lubricant retention.

The visual trend of the representative 2D roughness profiles, derived from the measured parameters, is consistent. The YSZ-

Table 7 EDS point analysis of the YSZ-coated SR34 steel sample

Point ID	C, wt.%	O, wt.%	Fe, wt.%	Y, wt.%	Zr, wt.%	Interpretation
YSZ-coated sample	32.69	24.44	34.22	6.25	2.40	Confirms local presence of yttria-stabilized zirconia coating; Fe originates mainly from substrate interaction due to thin coating thickness.

Table 8 Surface roughness parameters of uncoated, YSZ-coated, and CSZ-coated SR34 steel (mean ± standard deviation)

Sample	Rp, μm	Rv, μm	Rz, μm	Rc, μm	Rt, μm	Ra, μm	Rq, μm
Uncoated SR34	0.851 ± 0.041	0.922 ± 0.045	1.77 ± 0.09	0.728 ± 0.036	2.06 ± 0.11	0.274 ± 0.018	0.333 ± 0.020
YSZ-coated SR34	0.829 ± 0.038	0.707 ± 0.032	1.54 ± 0.08	0.743 ± 0.035	1.75 ± 0.09	0.235 ± 0.015	0.286 ± 0.018
CSZ-coated SR34	0.542 ± 0.029	0.933 ± 0.046	1.47 ± 0.07	0.545 ± 0.028	1.68 ± 0.08	0.188 ± 0.012	0.247 ± 0.015

coated profile (Fig. 8) is flatter and has a lower amplitude, though it still shows high peaks. The CSZ-coated profile (Fig. 9) has the least height variation and a reduced amplitude envelope. The representative 3D surface maps also show a gradual transition from the relatively rough uncoated topography to the smoother topography of the coated sample, with the CSZ-coated sample exhibiting the best uniformity in the topographical field. These reconstructions are consistent with the numerical trend and provide a useful visual summary of the manuscript.

In functional terms, the observed reduction in roughness is important for top piston ring applications. Contact between piston rings and the cylinder liner is highly sensitive to surface finish because asperity intensity and pattern directly determine initial contact mechanics, friction, and wear. Reduced roughness tends to promote a more stable running-in period and reduce the likelihood of intense asperity interactions, particularly when paired with a hard ceramic surface layer. Thus, the reduced roughness of the CSZ coating, and subsequently the YSZ coating, indicates that the coating enhances the surface integrity of SR34 steel and that the CSZ coating provides the greatest improvement in topographic smoothness on its own.

3.5 Microhardness Analysis

The Vickers indentation results show the apparent surface/composite hardness of the uncoated and coated SR34 systems. Because the YSZ and CSZ coatings were only approximately 1 μm thick, the measured hardness values of the coated samples may include contributions from both the ceramic coating and the underlying SR34 substrate. Therefore, these values should not be interpreted as the intrinsic hardness of the isolated coating layers. Instead, they provide a comparative indication of the resistance of the coated surface systems to indentation under the selected test conditions. The mean apparent hardness (Fig. 10) of the uncoated SR34 substrate was 390.4 HV, whereas the CSZ-coated and YSZ-coated SR34 specimens showed higher apparent hardness values of 614.54 HV and 668.54 HV, respectively. Although the coated samples exhibited significantly higher hardness than the uncoated substrate, interpret the measured values carefully because the coating thickness (~1 μm) is comparable to the deformation scale produced during Vickers indentation. The indentation response therefore extends beyond the ceramic layer and includes a contribution from the SR34 substrate. The measured hardness increase indicates that the deposited zirconia layers provide enhanced resistance against surface indentation and deformation; however, the reported values represent the overall mechanical response of the coating/substrate system rather than the intrinsic hardness of YSZ or CSZ.

The substrate influence also explains the variation observed among individual indentation measurements. The YSZ-coated sample exhibited a higher standard deviation (59.91 HV) compared with CSZ (21.93 HV), which may result from local differences in coating thickness, coating morphology, and the varying contribution of the underlying substrate during indentation. Therefore, while YSZ showed the highest apparent hardness, further nanoindentation analysis is needed to determine the true hardness and elastic properties of the individual coating layers. This corresponds to 57.41 and 71.24% increases in hardness for CSZ and YSZ, respectively, over the bare substrate. This trend indicates that EB-PVD deposition of stabilized zirconia coatings increased the indentation resistance of the SR34 surface system. Among the coated specimens, the YSZ-coated sample exhibited the highest apparent hardness, followed by the CSZ-coated sample and the uncoated SR34 substrate.

The five-point hardness profile also showed that the substrate had the least variation (Table 9), while the YSZ-coated sample showed greater point-to-point scatter. The standard deviation values were 12.50 HV for the substrate, 21.93 HV for CSZ, and 59.91 HV for YSZ. Such behavior is understandable in thin ceramic coatings, since local hardness can depend on variations in coating thickness, non-uniformity in microstructure, and the partial contribution of the substrate during indentation (Ref 59). However, the general trend is evident that both coatings increased the surface hardness of SR34 steel, with YSZ exerting the greatest hardening effect. This enhancement is significant in piston ring applications, where increased surface hardness can improve wear resistance, reduce plastic deformation, and enhance resistance to surface damage during operation.

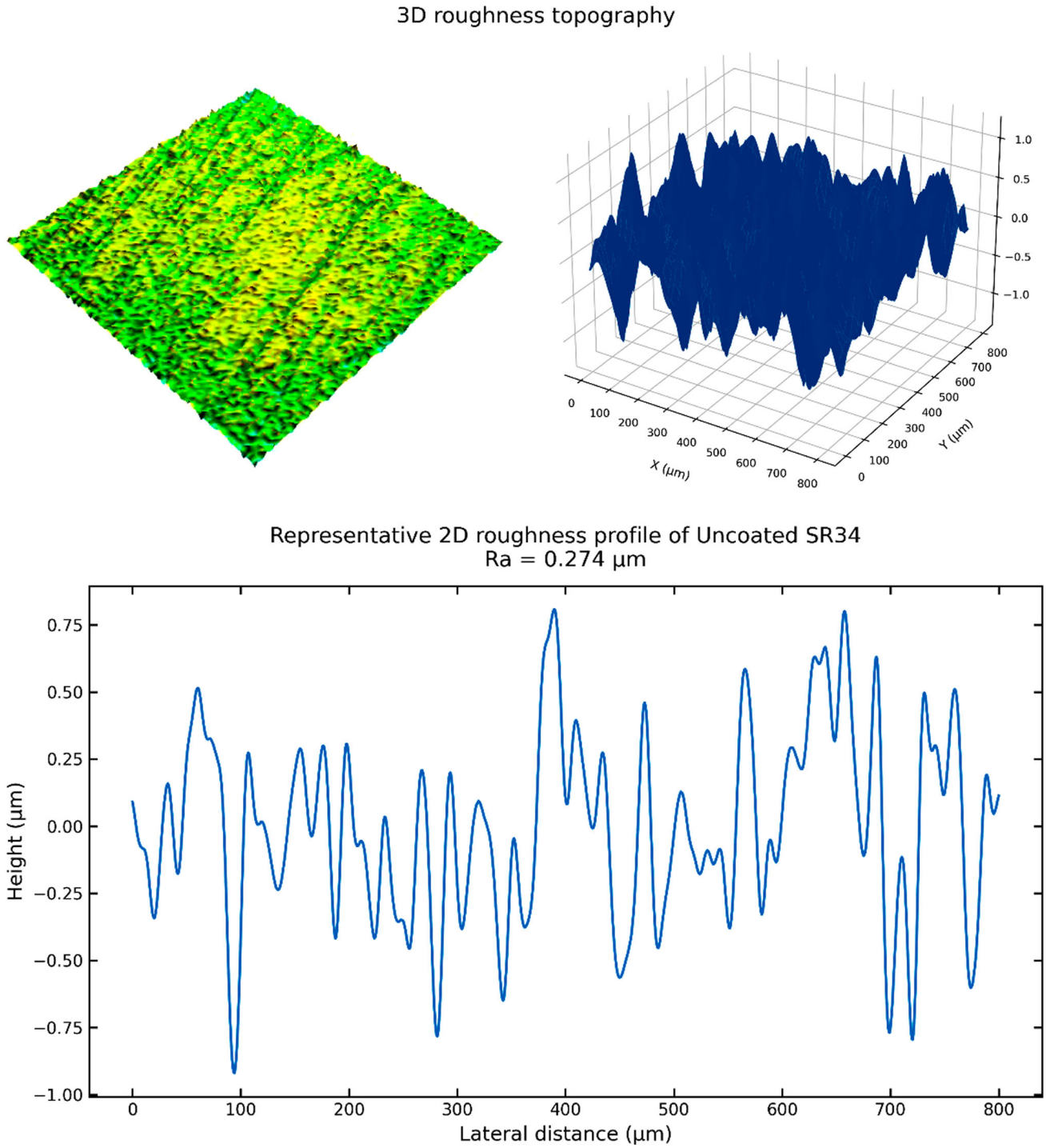


Fig. 7 Representative 3D surface map, 2D surface topography, and line profile of the roughness morphology of uncoated SR34

3.6 Sliding Wear Analysis

The uncoated SR34 steel, YSZ-coated SR34, and CSZ-coated SR34 samples were evaluated using a pin-on-disk tribometer under lubricated sliding conditions against a cast iron counterface. All three specimen groups were tested at both 5 and 10 kg loads at a constant rotational speed of 900 rpm for 900 s. The wear behavior was evaluated using weight loss, specific wear rate, and coefficient of friction. The results show that both zirconia-based coatings significantly improved the sliding wear performance of SR34 steel, with the CSZ-coated sample showing the lowest weight loss, wear rate, and coefficient of friction under the present laboratory testing conditions.

At 5 kg, the uncoated substrate lost 0.002409 g, and the CSZ- and YSZ-coated substrates lost 0.000066 and 0.000112 g, respectively, as shown in Table 10. This implies that the CSZ coating reduced wear loss by approximately 97.26%, while the YSZ coating reduced it by approximately 95.35%, compared to the uncoated substrate. The same trend was observed at 10 kg. The uncoated sample showed the

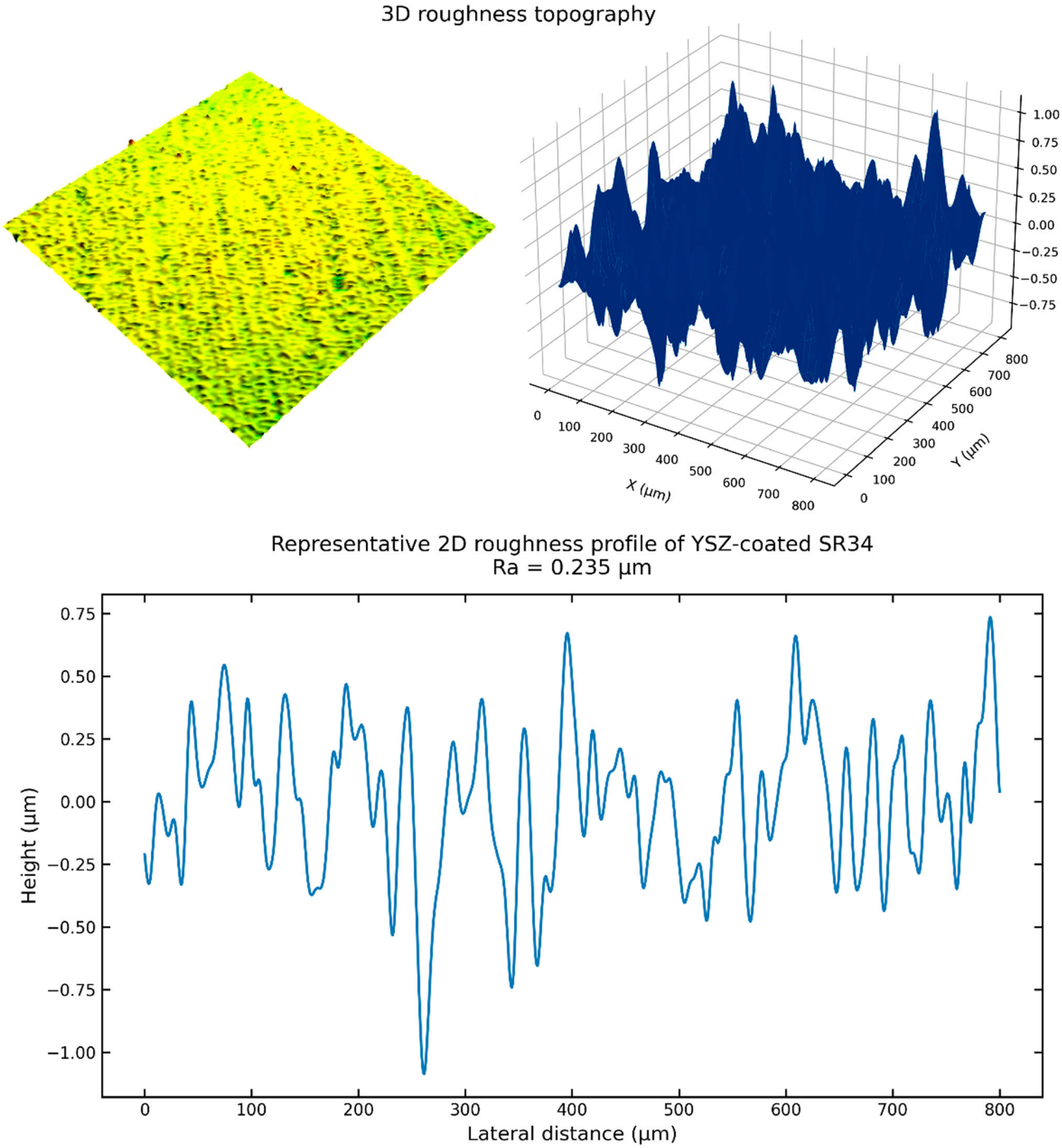


Fig. 8 Representative 3D surface map, 2D surface topography, and line profile of the roughness morphology of YSZ-coated SR34

highest weight loss (0.004293 g), while the CSZ and YSZ coatings reduced it to 0.000132 and 0.000336 g, corresponding to 96.93% and 92.17% loss, respectively. These findings indicate that the ceramic coating offered high resistance to mass loss, and the CSZ coating best maintained this resistance even at high load.

The individual wear rate of the uncoated SR34 sample was approximated from the experimental mass loss data in Table 11. The values were 7.48×10^{-7} mm^3/Nm at 5 kg and 6.67×10^{-7} mm^3/Nm at 10 kg. These values are significantly higher than those of the coated samples, demonstrating the bare SR34 surface's high wear vulnerability under lubricated sliding. Compared with the uncoated substrate, the CSZ coating reduced the specific wear rate by approximately 96.5% at 5 kg and 96.0% at 10 kg, whereas the YSZ coating reduced it by approximately 94.0% and 89.9%, respectively. Compared with CSZ and YSZ, the uncoated wear rate was nearly 28.3 times greater at 5 kg and 16.7 times greater at 10 kg. The wear rate data for the coated samples, in particular, support this conclusion. For the CSZ-coated sample, the wear rate was 2.643885×10^{-8} mm^3/Nm at 5 kg and 2.643869×10^{-8} mm^3/Nm at 10 kg. The nearly constant value indicates

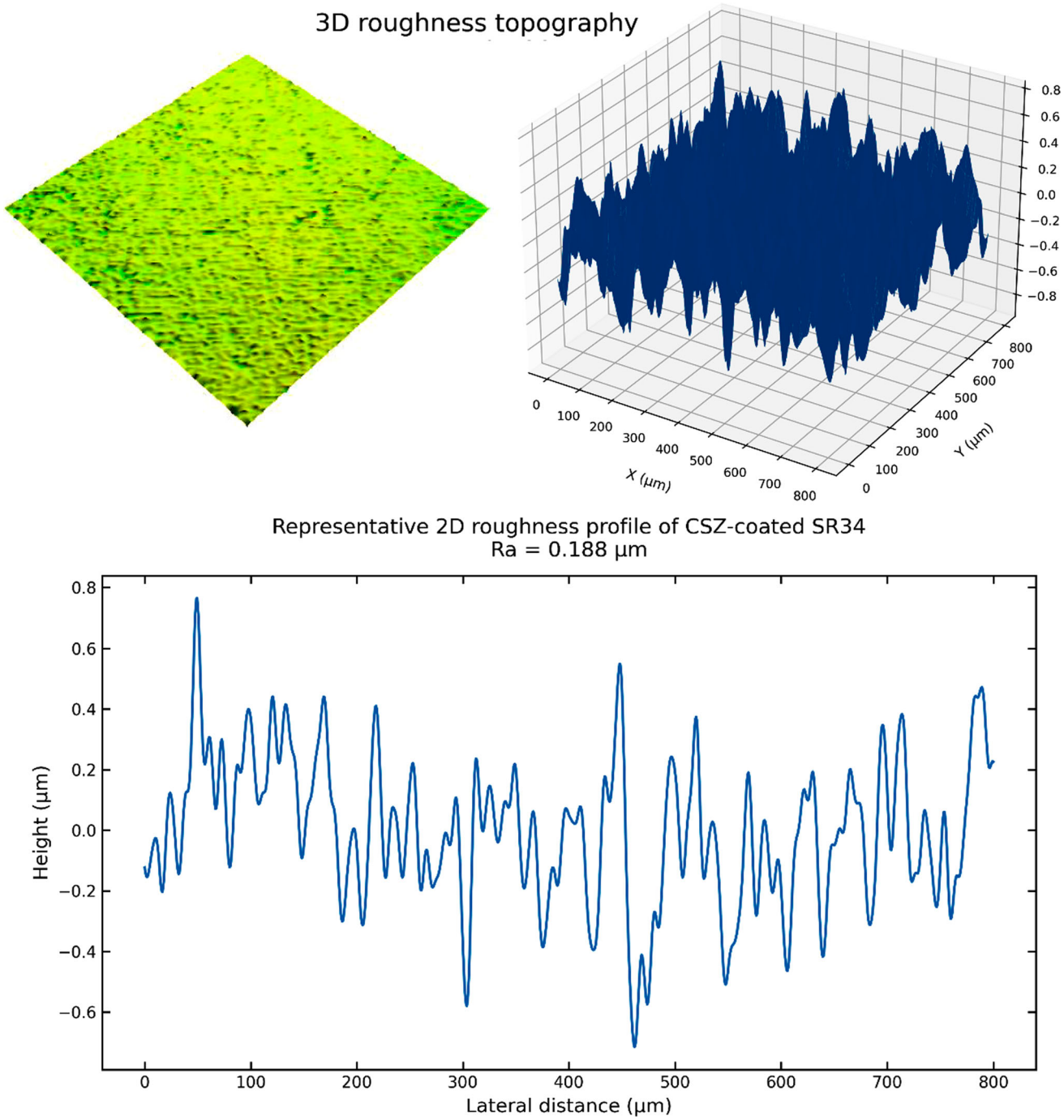


Fig. 9 Representative 2D surface map, 3D surface topography, and line profile of the roughness morphology of CSZ-coated SR34

extremely steady tribological behavior and suggests that the CSZ coating retained its protective properties even when the normal load was doubled. Conversely, the YSZ-coated sample exhibited a wear rate of 4.486493×10^{-8} mm^3/Nm at 5 kg and 6.729889×10^{-8} mm^3/Nm at 10 kg, indicating that the YSZ wear rate is more sensitive to load than CSZ. The CSZ coating had a lower wear rate than YSZ under both loading conditions.

The coefficient of friction results also align with the wear data, and Fig. 11 plots the COF curve over time. The average COF of the uncoated SR34 sample was 0.51 at 5 kg and 0.67 at 10 kg, much higher than that of the coated samples. By comparison, the CSZ-coated sample had average COF values of 0.144 at 5 kg and 0.130 at 10 kg, and the YSZ-coated sample had 0.147 at 5 kg and 0.142 at 10 kg. As a result, both coatings showed a drastic reduction in friction compared to uncoated SR34. The coefficient of friction decreased by about 71.8 percent in CSZ and 71.2 percent in YSZ, respectively, compared to uncoated SR34 at 5 kg. The decrease was even higher at 10 kg, with CSZ and YSZ showing approximately 80.6 percent and 78.8 percent decreases, respectively. These values clearly demonstrate that the uncoated substrate exhibited significantly greater interfacial resistance to sliding, whereas the ceramic-coated surfaces provided a more stable, lubricated tribological interface.

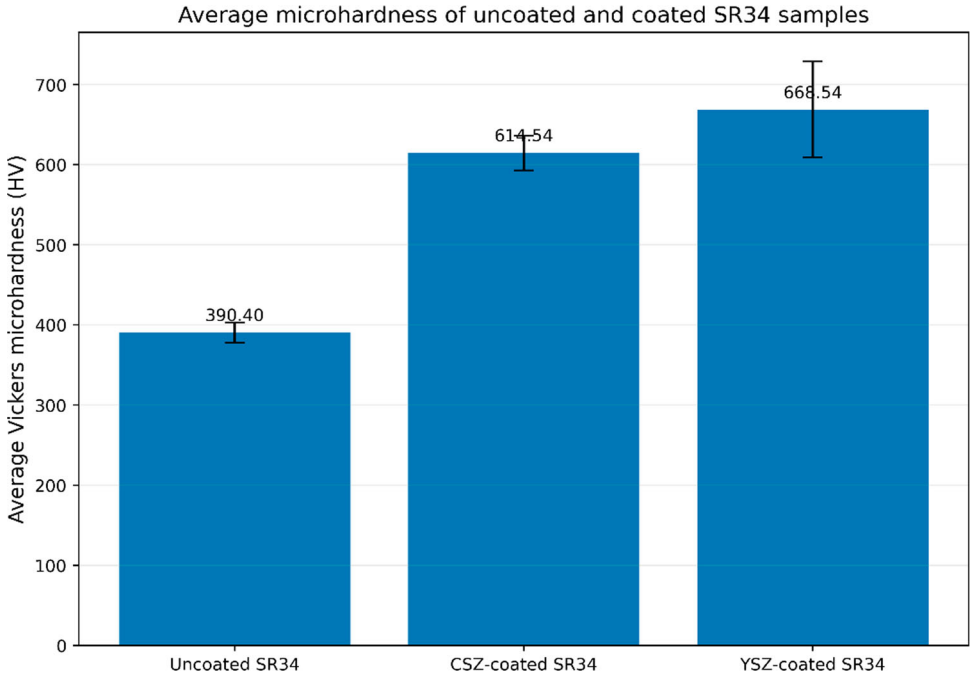


Fig. 10 Microhardness profile of uncoated SR34, CSZ-coated SR34, and YSZ-coated SR34 measured at five indentation locations

Table 9 Apparent composite Vickers hardness of uncoated and coated SR34 samples measured at five locations

S. No.	Uncoated SR34, HV	CSZ-coated SR34, HV	YSZ-coated SR34, HV
1	382.0	649.0	662.6
2	410.0	622.0	755.2
3	386.0	608.5	692.4
4	379.0	596.6	596.6
5	395.0	596.6	635.9
Average	390.40	614.54	668.54
Standard deviation	12.50	21.93	59.91

Table 10 Weight loss of uncoated and coated SR34 specimens after lubricated sliding wear testing at 5 kg and 10 kg

		5 kg			10 kg		
S.NO	Material	Before, grams	After, grams	Weight loss, grams	Before, grams	After, grams	Weight loss, grams
1	CSZ	1.047802	1.047736	0.000066	1.076966	1.076834	0.000132
2	YSZ	1.065178	1.065066	0.000112	1.035918	1.035582	0.000336
3	UNCOATED	1.035648	1.033239	0.002409	1.021743	1.01745	0.004293

Table 11 Wear rate and coefficient of friction of uncoated and coated SR34 specimens under lubricated sliding at 5 kg and 10 kg

		Wear Rate, mm^3/Nm		COF	
S.NO	Material	5Kg,	10Kg,	5Kg,	10Kg,
1	CSZ	$2.643885X10^{-8}$	$2.643869X10^{-8}$	0.144	0.130
2	YSZ	$4.486493X10^{-8}$	$6.729889X10^{-8}$	0.147	0.142
3	Uncoated	7.48×10^{-7}	6.67×10^{-7}	0.51	0.67

Another aspect of interest is the load dependence of friction. The COF of the uncoated sample increased from 0.51 to 0.67 between 5 and 10 kg, a percentage change of approximately 31.4. This indicates that tribological performance is not steady and that asperity interaction intensifies at higher loads. Conversely, the CSZ-coated sample reduced its COF from 0.144 to 0.130, whereas the YSZ-coated sample had a smaller reduction from 0.147 to 0.142, or 3.40. Although the uncoated substrate became more friction-prone as the load increased, the coated samples, especially CSZ, showed better load accommodation and more consistent sliding behavior.

The previous hardness and roughness results can be linked to the coatings' tribological superiority. The uncoated substrate had the highest roughness and the lowest hardness, consistent with the maximum wear loss. Coatings YSZ and CSZ significantly improved surface appearance, though their contributions appear to differ. The YSZ-coated sample had the highest microhardness, indicating greater resistance to localized penetration and plastic deformation. However, the CSZ-coated sample exhibited the lowest surface roughness and the best wear performance. This implies that, in lubricated sliding against cast iron, tribological performance cannot be determined solely by hardness. Rather, the CSZ coating seems to strike a favorable balance among surface smoothness, interfacial stability, and coating integrity. That is, the smoother CSZ surface probably reduced real asperity contact more effectively, leading to lower friction and less wear, even though it was slightly softer than YSZ.

The wear performance of the coated samples can be attributed to the combined influence of coating microstructure, hardness, and surface topography. SEM observations confirmed that both YSZ and CSZ coatings formed continuous and adherent ceramic layers without visible delamination or through-thickness cracking. The compact EB-PVD coating structure provided an effective protective barrier between the cast iron counterface and the SR34 substrate, thereby reducing direct metallic contact and suppressing severe adhesive wear mechanisms. The microhardness results indicate that the YSZ-coated sample exhibited the highest apparent hardness (668.54 HV), followed by CSZ (614.54 HV), demonstrating improved resistance against indentation and plastic deformation compared with uncoated SR34 (390.4 HV). YSZ's higher hardness contributed to improved resistance to localized deformation; however, hardness alone did not determine overall wear performance.

CSZ's superior wear behavior mainly resulted from its lower surface roughness (Ra = 0.188 μm) than YSZ (Ra = 0.235 μm) and uncoated SR34 (Ra = 0.274 μm). The smoother CSZ surface reduced asperity interaction, minimized plowing action against the counterface, and promoted more stable lubricated sliding conditions. Therefore, although YSZ possessed higher hardness, the optimized combination of surface smoothness, coating integrity, and adequate hardness enabled CSZ to achieve lower friction and wear loss. These observations indicate that a balance between mechanical strengthening and interfacial contact behavior governed the wear mechanism of the zirconia-coated samples. The uncoated SR34 experienced severe adhesive and abrasive wear due to its lower hardness and higher surface roughness. In contrast, the ceramic coatings reduced direct contact damage by providing a hard, smooth, and chemically stable sliding surface.

Overall, the sliding wear results indicate the following performance sequence under the current test conditions: CSZ-coated SR34 > YSZ-coated SR34 > uncoated SR34. At 5 kg and 10 kg, the CSZ coating recorded the lowest weight loss, wear rate, and coefficient of friction. The YSZ coating showed significantly better wear resistance than the uncoated substrate, and its wear rate and friction were also more favorable than those of CSZ, especially at higher loads. These results indicate that although both coatings can be used in top piston ring applications, the CSZ coating exhibited the best tribological response during lubricated sliding between the coating and cast iron in the current study.

3.7 Abrasion Resistance Analysis

The microabrasion test was conducted on CSZ- and YSZ-coated SR34 steel samples under controlled conditions to determine the abrasion resistance of these alloys. The test used a 25-mm-diameter HCHCR steel ball to initiate wear on the coated surface. The samples were subjected to a normal load of 20 N and rotated at 300 rpm for 20 min. The abrasive medium was a diamond suspension to provide uniform, high-intensity surface wear. The wear path created during this test is essential for determining coating stability in an actual tribological environment, where abrasive contacts occur in most cases.

The VMS images of the wear track on the (Fig. 12a) CSZ and (Fig. 12b) YSZ coatings are shown in Fig. 12. These images clearly show significant wear on the coated area, and both coatings exhibit material loss due to rolling fatigue from the steel ball's constant movement. The images reveal that both coatings (CSZ and YSZ) still exhibit clear wear patterns, and no delamination or peeling is apparent between the substrate and the coatings. This is an important observation, indicating that the coatings adhered well to the SR34 substrate during the wear test and that no significant interfacial damage was observed under the test conditions.

The wear track images can also be used to determine the coating area and the underlying substrate. In both cases, the coating is visibly thinner where it has worn off, while the substrate beneath remains intact, indicating that the wear was primarily on the ceramic coating. No evidence of substantial wear in the substrate area indicates that the coatings successfully shielded the SR34 steel from direct abrasive contact. Constant rolling wear of the ball on the coating gradually reduced coating thickness without causing major structural failure or peeling.

3.7.1 Coating Thickness Measurement and Analysis. The abrasion test results were used to determine the coating thicknesses of the CSZ and YSZ coatings, as shown in Table 12. The wear track formed during the test was analyzed to determine the thickness. The coating thickness obtained from the micro-abrasion crater analysis was evaluated using multiple measurements. The CSZ coating exhibited an average thickness of 1.21 $\pm$ 0.06 μm, whereas the YSZ coating showed an average thickness of 1.04 $\pm$ 0.05 μm. The obtained standard deviations indicate good thickness uniformity and reproducibility of the EB-PVD deposition process. These values are consistent with typical thin coatings produced by EB-PVD processes and indicate that both coatings were successfully deposited on the SR34 substrate without excessive deposition, which is desirable for top piston rings that demand high dimensional accuracy.

Although the coating thicknesses differed slightly, the CSZ and YSZ coatings were highly protective of the SR34 steel, as evidenced by minimal substrate wear. The coating thicknesses are already within the anticipated range for tribological applications, which require a thin yet tough coating that provides wear protection without compromising dimensional integrity. The coating–substrate interface did not peel or delaminate during the test, and the results clearly

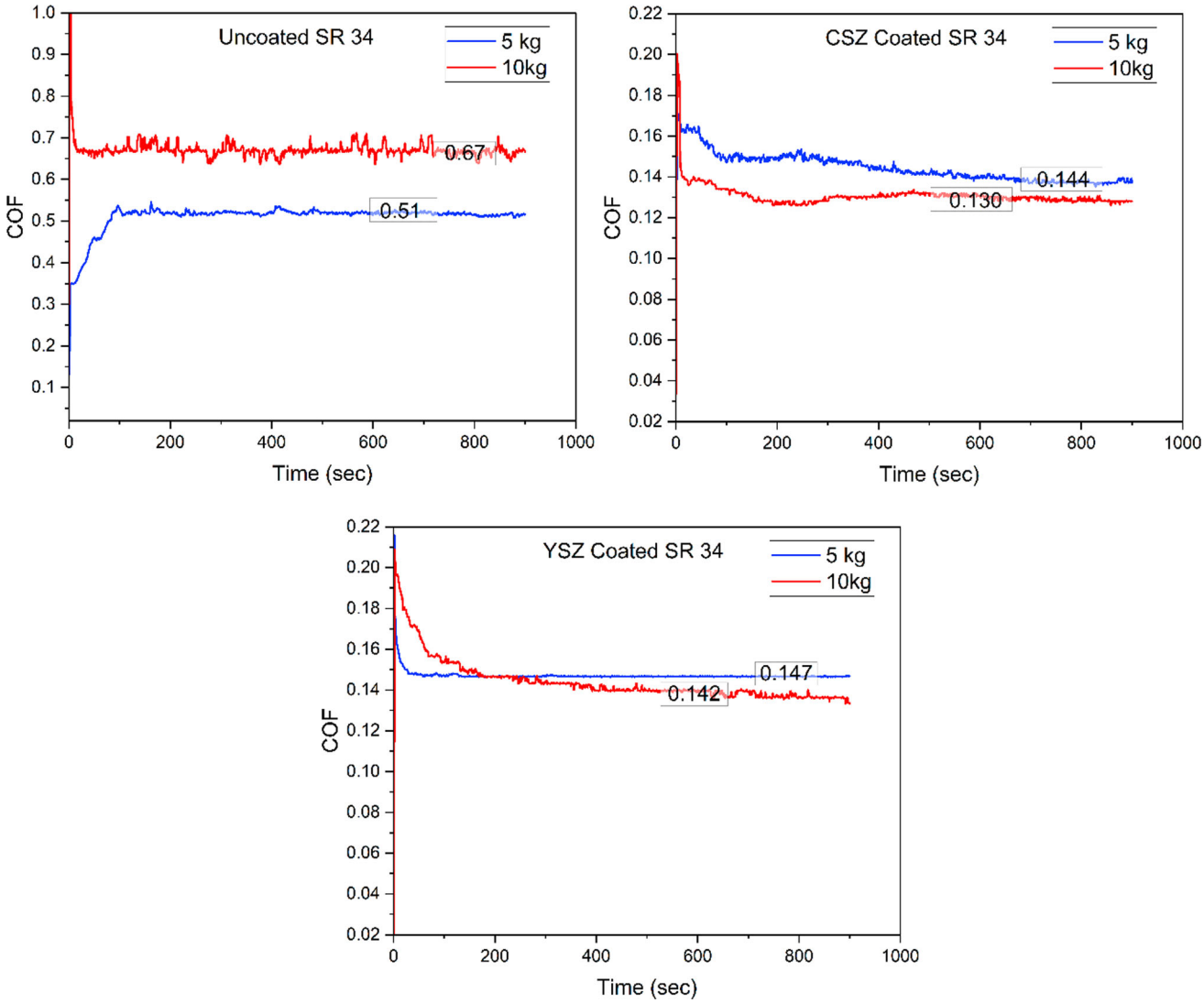


Fig. 11 Coefficient-of-friction curves of (a) uncoated SR34, (b) CSZ-coated SR34, and (c) YSZ-coated SR34 under lubricated sliding conditions

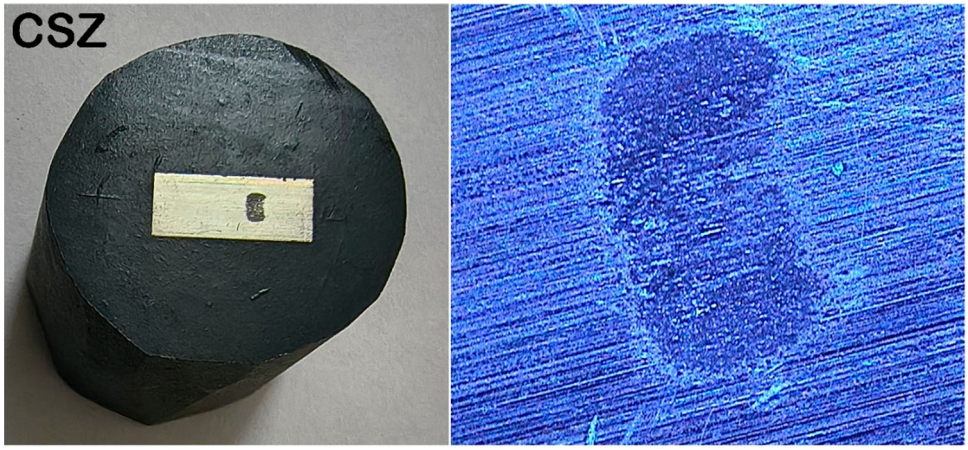
indicate the coatings' good adhesion and stability under abrasive conditions.

3.8 Dilatometer Testing and Thermal Expansion Analysis

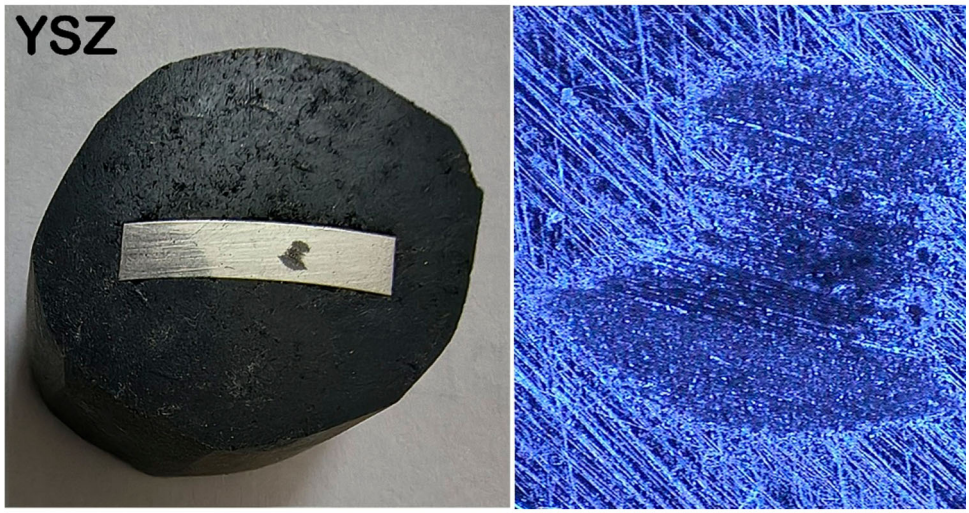
A dilatometer was used to measure the coefficient of thermal expansion (CTE) of the uncoated SR34 steel and its respective coatings, CSZ and YSZ, to assess their dimensional stability under temperature variations. Figure 13 shows the temperature–CTE curves for coated and uncoated SR34 samples. The CTE values of the substrate and the two coatings at 5 °C are summarized in Table 13.

From Table 13, the uncoated SR34 substrate exhibited a CTE of 1.01×10^{-5} °C^{-1}. This is within the acceptable range for SR34 steel (1.00×10^{-5} to 1.20×10^{-5} °C^{-1}). The coated samples had a CTE slightly higher than the substrate, with CSZ at 1.07×10^{-5} °C^{-1} and YSZ at 1.06×10^{-5} °C^{-1}. The values are quite close to the substrate CTE, indicating that the coatings are thermally compatible with the SR34 steel substrate. The similar CTE values between the coating and the SR34 substrate indicate that, across varying temperatures, the coated SR34 samples should exhibit good thermal compatibility. Keep this in mind when using it in applications likely to experience high temperatures or thermal cycling, such as engine components like piston rings. As shown in the temperature vs. CTE plot, all three materials (uncoated SR34, CSZ-coated SR34, and YSZ-coated SR34) exhibited a fairly constant CTE with only slight variation with temperature. This shows that the coatings do not cause major thermal expansion differences between the coatings and substrate that would otherwise cause stresses or delamination during thermal cycling. The thermal expansion characteristics of the coated samples fell within an acceptable range for SR34 steel in thermal applications, ensuring the coating will not negatively impact the substrate's performance under temperature changes. Thus, the CSZ and YSZ coatings are thermally stable and can be used in high-temperature applications (such as engine parts) where thermal expansion compatibility is paramount to prevent failure or degradation.

Overall, the dilatometry data suggest that both CSZ and YSZ overlayer materials are thermally compatible with the SR34 substrate, as their CTE values are similar. The CTE increment of the coatings relative to the substrate is negligible and would not pose a problem due to thermal expansion



(a)



(b)

Fig. 12 (a) VMS image of the wear track produced on the CSZ-coated sample (b) VMS image of the wear track produced on the YSZ-coated sample

Table 12 Coating thickness of CSZ and YSZ coatings

Material	Distance(X), mm	Distance(Y), mm	Diameter of Ball, mm	Coating Thickness, μm
CSZ	8.4	3.6	25	1.2096 ± 0.06
YSZ	7.9	3.3	25	1.0428 ± 0.05

mismatches. The coatings are likely to work well in high-temperature applications without introducing thermal strains, since the CTE range of SR34 steel is 1.00×10^{-5} to 1.20×10^{-5} at 5 °C. This renders the EB-PVD-coated SR34 steel suitable for applications where thermal expansion is critical, such as piston rings.

Overall, the findings indicate that EB-PVD deposition of YSZ and CSZ effectively altered the surface of SR34 steel, with particular applicability to the top piston ring application. FTIR and XRD confirmed the presence of stabilized zirconia-based ceramic coatings. SEM/EDS showed that both coatings were continuous, adherent, and chemically matched the intended YSZ and CSZ blends. The surface roughness decreased after CSZ coating, yielding the smoothest surface. Microhardness increased significantly after coating, with YSZ exhibiting the highest hardness. Sliding wear and friction tests showed that both coatings outperformed the uncoated substrate, with CSZ performing best overall tribologically. Abrasion testing confirmed good adhesion and coating continuity, and dilatometry confirmed good thermal compatibility between the coatings and the SR34 substrate. In conclusion, both YSZ and CSZ are viable EB-PVD ceramic coatings for SR34 piston ring steel, though their performance priorities differ slightly. YSZ was the hardest, while CSZ was the most balanced in terms of smoothness, low friction, low wear rate, abrasion resistance, and thermal compatibility. Under the current experimental

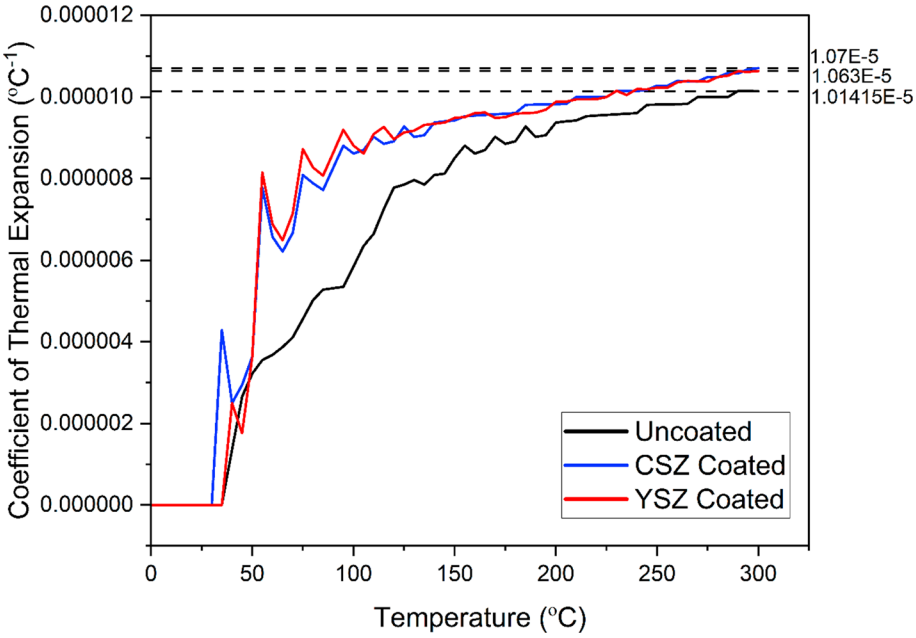


Fig. 13 Temperature vs. coefficient of thermal expansion (CTE) for uncoated, CSZ-coated, and YSZ-coated SR34

Table 13 Coefficient of thermal expansion of substrate and coating materials

S.NO	Material	Coefficient of thermal expansion, °C^{-1})
1	SUBSTRATE	1.01415 X 10^{-5}
2	CSZ	1.07 X 10^{-5}
3	YSZ	1.06 X 10^{-5}

conditions, CSZ appears to be the more desirable coating for improving the tribological behavior of the SR34 top piston ring material.

3.9 Tribocorrosion Behavior of Uncoated and Coated SR34 Samples

3.9.1 OCP–time Response during Tribocorrosion. An initial evaluation of the tribocorrosion response of uncoated SR34, YSZ-coated SR34, and CSZ-coated SR34 was conducted by examining the variation in open-circuit potential with time. Representative OCP–time curves are shown in Fig. 14. The curves show three distinct regions: a pre-sliding stabilization phase, a possible steep drop during sliding, and a post-sliding recovery phase after the contact was lifted. Before sliding, all samples stabilized at relatively constant open-circuit potentials. As sliding commenced, the potentials rapidly shifted toward more negative values, indicating depassivation or mechanical perturbation of the surface film/coating in the electrolyte. The greatest negative change was observed in the uncoated SR34 sample in Fig. 14, with smaller potential drops in the coated samples, confirming that zirconia coatings reduce mechanically induced electrochemical activation.

Figure 14 shows that the CSZ-coated surface had the lowest potential drop and the fastest post-sliding recovery among the coated surfaces, indicating that it better maintained its barrier properties during sliding and was more likely to repassivate sooner after contact termination. The YSZ-coated sample was also superior to the uncoated substrate but showed slightly worse potential drop and recovery characteristics than CSZ. The trend indicates that the CSZ interface was more stable under simultaneous wear and corrosion.

3.9.2 Tribocorrosion Polarization Behavior. Figure 15(a) shows representative tribocorrosion Tafel polarization behavior, and Table 14 summarizes the extracted electrochemical parameters. The uncoated SR34 sample had the lowest corrosion potential (− 548 mV vs SCE) and the highest corrosion current density (0.0613 mA/cm2), corresponding to a corrosion rate of 0.711 mmpy. Conversely, the YSZ-coated sample showed a significant change, with Ecorr = − 438 mV vs SCE and Icorr = 0.0174 mA/cm^2, yielding a corrosion rate of 0.202 mmpy. The CSZ-coated sample performed best overall, with Ecorr = − 409 mV vs SCE and Icorr = 0.0118 mA/cm^2, yielding a corrosion rate of 0.137 mmpy.

Both coated samples shifted the electrochemical response, as shown in Fig. 15(a), to a lower current density and a more noble corrosion potential than uncoated SR34. These values show that the tribocorrosion current density decreased by approximately 71.6% for YSZ and 80.8% for CSZ compared to the bare substrate. The change in Ecorr toward more noble potentials in the coated samples indicates that the ceramic coating interfered with the electrochemical reactivity of the SR34 surface, even during mechanically assisted degradation. Thus, the Tafel response confirms that the two coatings still maintained a significant barrier effect during sliding, although the protection level was lower than expected under pure corrosion conditions.

3.9.3 EIS Response under Tribocorrosion Conditions. Figure 15(b), (c) and (d) shows the electrochemical impedance response under tribocorrosion conditions, and Table 15 contains the extracted EIS parameters. Figure 15(b) (Nyquist plot) and Fig. 15(c), (d) (Bode magnitude and phase plots) reveals that the ranking of corrosion resistance remains the same: CSZ-coated SR34 > YSZ-coated SR34 > uncoated

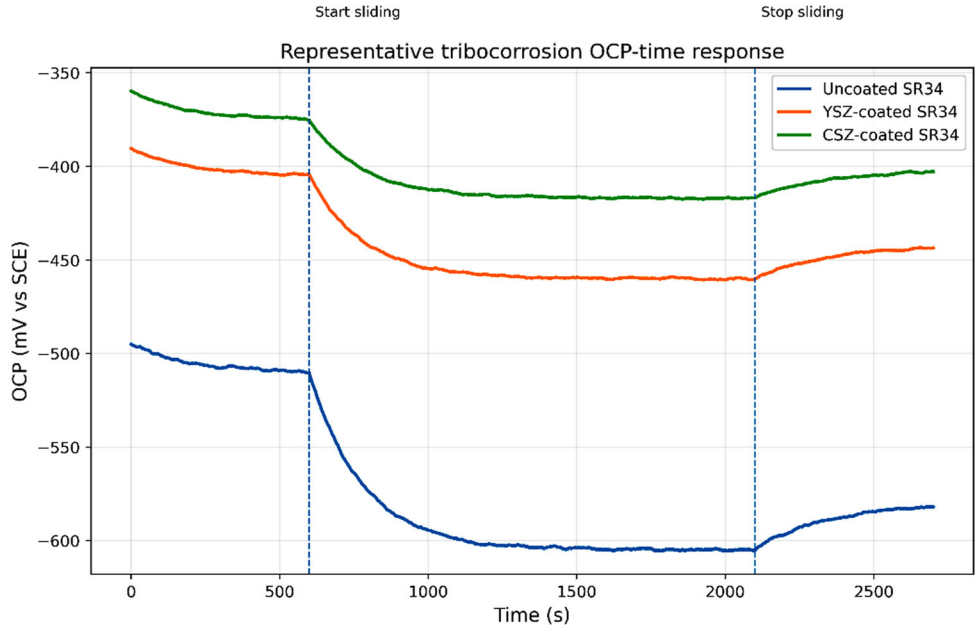


Fig. 14 Representative OCP–time response of uncoated, YSZ-coated, and CSZ-coated SR34 during tribocorrosion

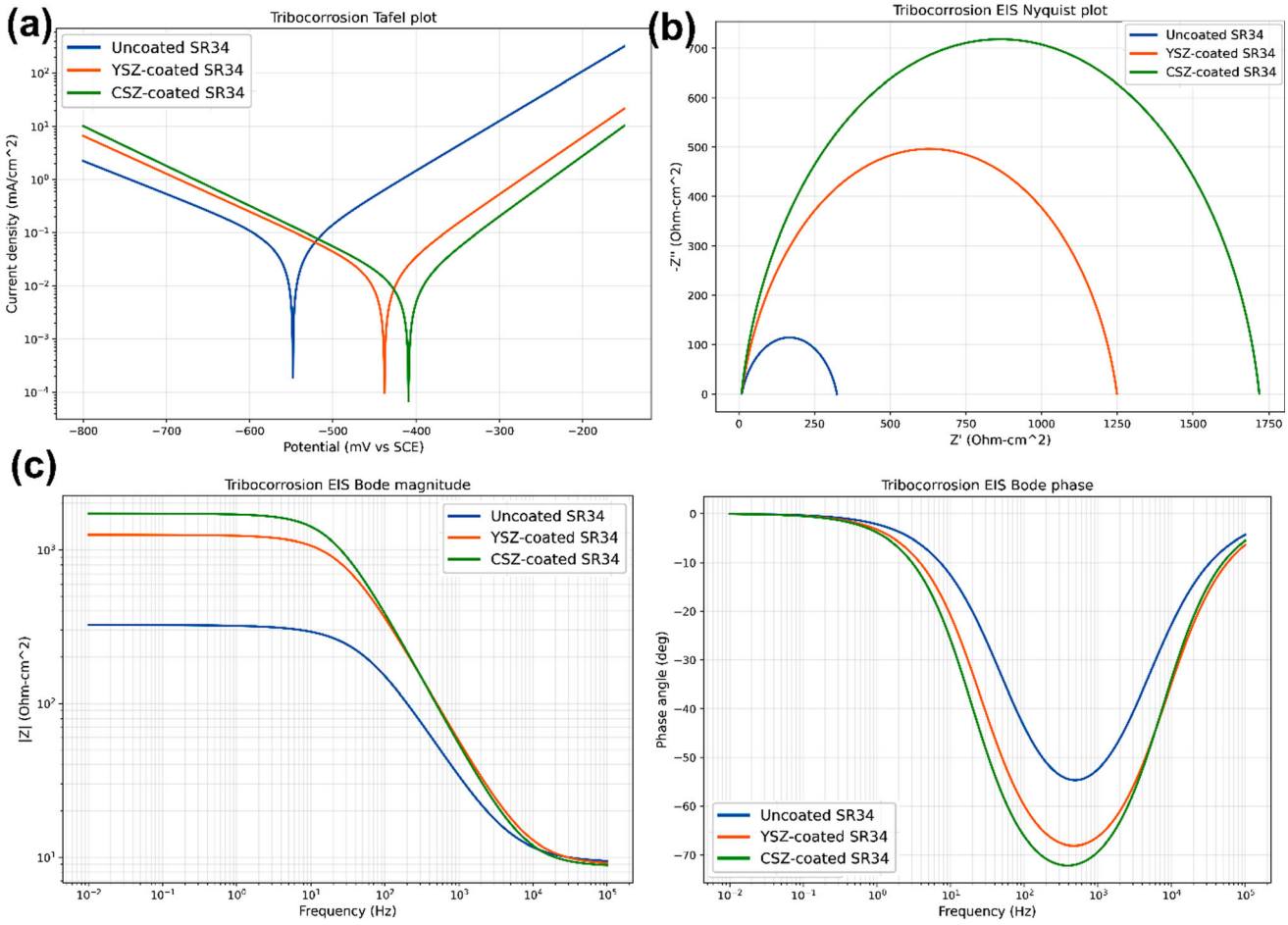


Fig. 15 Representative tribocorrosion electrochemical response of uncoated, YSZ-coated, and CSZ-coated SR34: (a) Tafel polarization plot, (b) EIS Nyquist plot, (c) EIS Bode magnitude plot, and (d) EIS Bode phase plot

Table 14 Representative tribocorrosion polarization parameters of uncoated and coated SR34 samples

Samples	Ecorr, mV SCE	Icorr, mA/cm^2	βa, mV/dec	βc, mV/dec	Corrosion rate, mmpy
Uncoated SR34	− 548	0.0613	107	161	0.711
YSZ-coated SR34	− 438	0.0174	93	140	0.202
CSZ-coated SR34	− 409	0.0118	88	133	0.137

Table 15 Representative tribocorrosion EIS parameters of uncoated and coated SR34 samples

Samples	Rs, Ω-cm^2	Rp, Ω-cm^2	Rct, Ω-cm^2	CPE, μp/cm^2
Uncoated SR34	9.2	430	315	268
YSZ-coated SR34	8.9	1530	1240	102
CSZ-coated SR34	8.7	2040	1710	74

SR34. The uncoated SR34 substrate had the lowest polarization resistance and charge transfer resistance (Rp = 430 Ω-cm^2 and Rct = 315 Ω-cm^2), and the largest CPE value (268 μp/cm^2), suggesting a highly active, non-uniform interface in tribocorrosion.

The impedance behavior of the YSZ-coated sample was better with Rp = 1530 Ω cm^2, Cpk = 1240 Ω-cm^2, whereas the CSZ-coated sample had the highest resistance values, that is, Rp = 2040 Ω-cm^2, Cpk = 1710 Ω-cm^2, and the lowest CPE of 74 μp/cm^2. The larger Nyquist semicircle of the CSZ-coated sample indicates higher resistance to charge transfer and electrolyte penetration than in YSZ and the uncoated substrate. Likewise, the higher impedance modulus at higher impedance and the more pronounced phase angle response indicate that CSZ maintained a more stable electrochemical interface during sliding.

The reduced CPE value of CSZ also indicates a less defective, more homogeneous tribocorrosion interface. Although the YSZ coating significantly enhanced the impedance response compared to the uncoated SR34, its resistance was still lower than that of CSZ. These results align with the overall tribological trend of this study, in which CSZ already exhibited the lowest roughness, the lowest friction, and optimal sliding wear characteristics. Figure 15(b, c and d) combines the EIS responses, indicating that CSZ displayed the best resistance to the coupled wear corrosion degradation process.

3.9.4 COF–time Behavior during Tribocorrosion. Figure 16 presents the representative coefficient-of-friction curves used during tribocorrosion. The uncoated SR34 sample had the highest friction during sliding, with significant variation and a large steady-state coefficient of friction. Conversely, in Fig. 16, both coated samples showed significantly lower and more stable COF behavior, indicating that the zirconia coating not only enhanced electrochemical stability but also interfacial resistance during sliding in a corrosive medium.

Figure 16 shows that the CSZ-coated sample has the lowest and smoothest COF response, compared with the YSZ-coated sample, which shows slightly higher friction and greater variation. This finding implies that the smoother surface and more stable interface of the CSZ coating reduce real asperity interactions more effectively than YSZ under tribocorrosion conditions. In this way, the COF–time response in Fig. 16 supports the electrochemical and EIS data, demonstrating that CSZ exhibits the most balanced wear and corrosion protection during simultaneous wear and corrosion. The combination of the OCP, polarization, impedance, and friction responses represented in Fig. 14, 15, and 16 demonstrates that tribocorrosion damage was most intense for the uncoated SR34 and least intense for the CSZ-coated sample. Figure 14 shows the largest negative OCP shift, Fig. 15(a) the highest corrosion current density, Figure 15(b), (c) and (d) the lowest impedance response, and Fig. 16 the highest friction during sliding of the uncoated substrate. The YSZ coating greatly enhances this behavior, although the CSZ coating exhibits the best overall performance.

Although the present tribocorrosion evaluation was performed in a controlled 3.5 wt.% NaCl environment, the results provide comparative information on the resistance of YSZ and CSZ coatings to simultaneous mechanical wear and electrochemical degradation. The NaCl electrolyte represents an aggressive aqueous corrosion medium and allows evaluation of the relative barrier performance of the coatings; however, it does not completely reproduce the actual operating conditions of piston rings in internal combustion engines. During engine operation, piston rings are exposed to elevated temperatures, reciprocating sliding motion, engine oil lubrication, lubricant oxidation products, fuel-derived contaminants, combustion gases, and intermittent corrosive species. These factors can influence coating degradation mechanisms through combined thermal, mechanical, and chemical effects. Therefore, the improved tribocorrosion resistance observed for CSZ and YSZ coatings in the present study should be considered as laboratory-scale comparative performance rather than direct prediction of engine service life. Future investigations should include high-temperature reciprocating tribocorrosion testing using engine oil-based lubricants or simulated combustion environments to further validate the suitability of EB-PVD zirconia coatings for practical piston ring applications

4. Conclusions

The present study successfully deposited YSZ and CSZ ceramic coatings on SR34 steel using EB-PVD and evaluated their suitability as protective coatings for top piston ring applications. The results confirmed the successful formation of continuous, adherent zirconia-based coatings with improved surface, mechanical, tribological, thermal, and tribocorrosion properties compared with uncoated SR34 steel. SEM/EDS

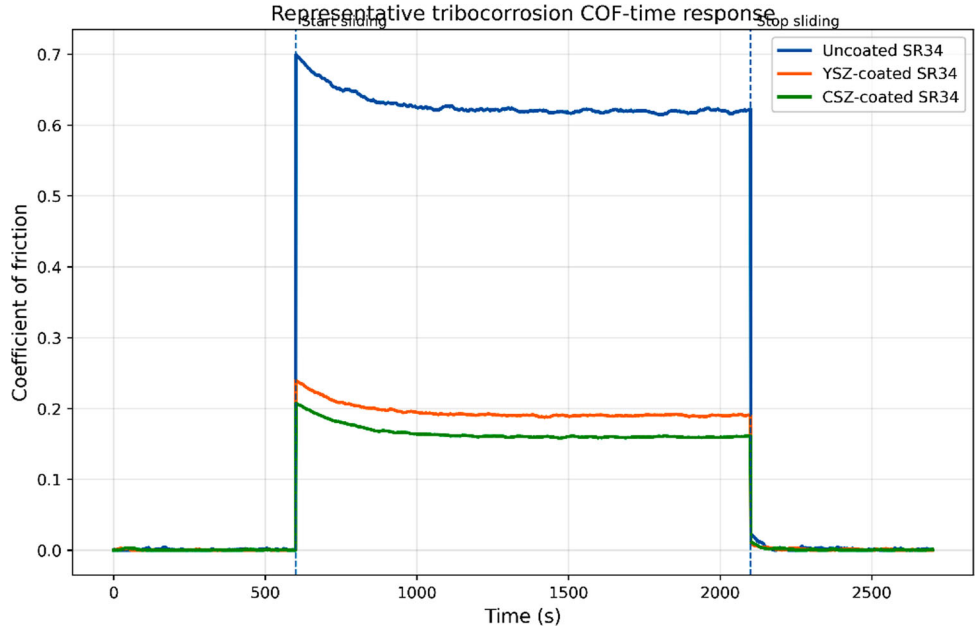


Fig. 16 Representative coefficient-of-friction response of uncoated, YSZ-coated, and CSZ-coated SR34 during tribocorrosion

analysis confirmed the presence of the intended stabilized zirconia systems, while the detected carbon signals were attributed to preparation-related contamination and electron interaction effects associated with the thin coating thickness rather than coating composition. XRD confirmed zirconia-based phase formation; however, quantitatively separating tetragonal and cubic zirconia phases requires further high-resolution analysis using Rietveld refinement or PDF database matching.

Both coatings reduced surface roughness compared with uncoated SR34, with CSZ exhibiting the lowest Ra value (0.188 μm), followed by YSZ (0.235 μm) and uncoated SR34 (0.274 μm). The microhardness results showed higher apparent composite hardness for coated specimens, with YSZ exhibiting the highest value (668.54 HV) compared with CSZ (614.54 HV) and the substrate (390.4 HV). These values represent the combined response of the coating/substrate system because the coating thickness ($\sim$1 μm) allows possible substrate contribution during Vickers indentation. Therefore, the hardness improvement indicates enhanced surface resistance but should not be considered the intrinsic hardness of the ceramic layers.

Under lubricated sliding against cast iron, both coatings significantly reduced wear loss, wear rate, and coefficient of friction compared with uncoated SR34. Although YSZ exhibited higher hardness, CSZ demonstrated superior overall tribological performance due to the combined effect of adequate hardness, smoother surface morphology, coating integrity, and reduced asperity-driven wear mechanisms. CSZ's lower roughness reduced interfacial contact severity and improved sliding stability. Abrasion testing confirmed good coating adhesion and resistance to coating failure, while thermal expansion analysis demonstrated compatibility between the zirconia coatings and the SR34 substrate. Tribocorrosion evaluation in 3.5 wt.% NaCl solution showed that both coatings improved resistance against coupled wear and electrochemical degradation, with CSZ providing the most stable response. However, the NaCl-based test represents a controlled laboratory environment and does not fully reproduce actual engine conditions involving high-temperature, lubricant interaction, combustion products, and reciprocating loading.

Overall, CSZ-coated SR34 exhibited the most balanced laboratory-scale performance among the investigated coatings, indicating strong potential for piston ring surface protection. Nevertheless, practical implementation requires further validation through high-temperature, reciprocating engine-simulated testing; lubricant-based tribocorrosion studies; long-duration durability evaluation; and full-scale piston ring testing. Future work should also include detailed crystallographic analysis using Rietveld refinement and PDF matching to accurately quantify zirconia phase fractions.

Author Contributions

Uthirapathy Chandrasekaran involved in investigation, writing—original draft. Hariharan K took part in research methodology; research administration; Saravanan Raju involved in formal analysis, writing—review & editing; Ilamvazhuthi C took part in visualization, writing—review & editing.

Funding

This research did not receive any specific funding.

Data Availability

No new data were generated in this study.

Conflict of interest

The authors declare that there are no conflicts of interest regarding the publication of this paper.

Ethical Approval

This study complies with ethical standards and does not involve human or animal subjects. The research is original, unpublished, and not under consideration elsewhere. All data and materials are generated by the authors or appropriately cited.

References

1. K. Suganeswaran, P. Muthukumar, R. Sathiskumar, R. Parameshwaran, and N. Nithyavathy, Evaluation of Microstructural, Tribological and Tensile Characteristics of AA7075 Surface Composites Fabricated through Friction Stir Process, *Proc. Inst. Mech. Eng. Part E J. Process Mech. Eng.*, IMECHE, 2023, p 09544089231170987, https://doi.org/10.1177/09544089231170987
2. A. Atulkar, R.K. Pandey, and P.M.V. Subbarao, Role of Textured Piston Rings/Liners in Improving the Performance Behaviours of IC Engines: a Review with Vital Findings, *Surf. Topogr. Metrol. Prop.*, 2021, **9**(2), 23002. https://doi.org/10.1088/2051-672X/ac0a36
3. S. Kumar and M.S. Charoo, Combined Effect of Laser Surface Texturing and CrCN Coating on the Friction between Piston Ring and Cylinder Liner Interface, *J. Mater. Eng. Perform.*, 2025, **34**(22), p 26894–26906. https://doi.org/10.1007/s11665-025-11267-6
4. J. Liu, Y. Zhang, and B. Liao, A Review on Preparation Process and Tribological Performance of Coatings for Internal Combustion Engine Piston Ring, *Adv. Mech. Eng.*, 2023, **15**(5), p 1–19.
5. K.G. Mahmoud, O. Knaus, T. Parikyan, G. Offner, and S. Sklepic, An Integrated Model for the Performance of Piston Ring Pack in Internal Combustion Engines, *Proc. Inst. Mech. Eng. Part K J. Multi-body Dyn.*, 2018, **232**(3), p 371–384. https://doi.org/10.1177/1464419317736676
6. S. Gai and J. Zhao, Simulation and Experimental Investigation on Fatigue Resistance of the Forged Steel Piston in High-Duty Engine, *J. Mater. Eng. Perform.*, 2023, **32**(7), p 3202–3214. https://doi.org/10.1007/s11665-022-07316-z
7. M.K.A. Ali, H. Xianjun, R.F. Turkson, and M. Ezzat, An Analytical Study of Tribological Parameters between Piston Ring and Cylinder Liner in Internal Combustion Engines, *Proc. Inst. Mech. Eng. Part K J. Multi-body Dyn.*, 2016, **230**(4), p 329–349. https://doi.org/10.1177/1464419315605922
8. S. Kumar and M. Kumar, Tribological and Mechanical Performance of Coatings on Piston to Avoid Failure—A Review, *J. Fail. Anal. Prev.*, 2022, **22**(4), p 1346–1369. https://doi.org/10.1007/s11668-022-01436-3
9. Y. Wu, C. Ma, H. Liu, G. Zang, and F. Du, Effect of Microarc Oxidation Power Frequency on the Tribological Performance of Amino-Modified Coatings with MoS2 Lubrication, *J. Mater. Eng. Perform.*, 2026 https://doi.org/10.1007/s11665-026-13800-7
10. F. Zhu, J. Xu, X. Han, Y. Shen, and M. Jin, Tribological Performance of Three Surface-Modified Piston Rings Matched with Chromium-Plated Cylinder Liner, *Ind. Lubr. Tribol.*, 2017, **69**(2), p 276–281. https://doi.org/10.1108/ILT-11-2015-0164
11. R. Ferreira, J. Martins, Ó. Carvalho, L. Sobral, S. Carvalho, and F. Silva, Tribological Solutions for Engine Piston Ring Surfaces: An Overview on the Materials and Manufacturing, *Mater. Manuf. Process.*, 2020, **35**(5), p 498–520. https://doi.org/10.1080/10426914.2019.1692352
12. O Özbek and N Altan Özbek (2025), Impact of Deep Cryogenic Treatment on X210CrW12 Steel's Wear Behavior and Microstructural Characteristics, Materials (Basel), 18, 4, 1, 20
13. R. Sri Siva, D. Mohan Lal, and M.A. Jaswin, Optimization of Deep Cryogenic Treatment Process for 100Cr6 Bearing Steel using the Grey-Taguchi Method, *Tribol. Trans.*, 2012, **55**(6), p 854–862. https://doi.org/10.1080/10402004.2012.720002
14. J.D. Darwin, D. Mohan Lal, and G. Nagarajan, Optimization of Cryogenic Treatment to Maximize the Wear Resistance of 18% Cr Martensitic Stainless Steel by Taguchi Method, *J. Mater. Process. Technol.*, 2008, **195**(1), p 241–247. https://doi.org/10.1016/j.jmatprotec.2007.05.005
15. D. Galeazzi, R.HGe. Silva, A.B. Viviani, P.R. Jaeger, and M.B. Schwedersky, Evaluation of Thermal and Geometric Properties of Martensitic Stainless Steel Thin Walls Built by Additive Manufacturing Cold Metal Transfer (CMT) Processes, *Int. J. Adv. Manuf. Technol.*, 2022, **120**(3–4), p 2151–2165. https://doi.org/10.1007/s00170-022-08921-x
16. S. Sengottaiyan, V.S. Shaisundaram, M.S. Basha, B. Deepanraj, and N. Senthilkumar, Effect of Duplex and Austenite Stainless Steel Fillers on Mechanical, Microstructural, and Corrosion Characteristics of Dissimilar Welds Using Cold Metal Transfer Welding, *Results Eng.*, 2025 https://doi.org/10.1016/j.rineng.2025.104818
17. N. Jeyaprakash, C.H. Yang, and S.P. Tseng, Wear Tribo-performances of Laser Cladding Colmonoy-6 and Stellite-6 Micron Layers on Stainless Steel 304 using Yb:YAG Disk Laser, *Met. Mater. Int.*, 2021, **27**(6), p 1540–1553. https://doi.org/10.1007/s12540-019-00526-6
18. S. Saravanan, S. Sengottaiyan, R. Aravind, and S. Krishnakumar, Assessment of the Tribological Behavior of WAAM-fabricated SS316L through Advanced Ensemble Machine Learning Predictions and RSM-based Optimization, *J. Mater. Eng. Perform.*, 2026, **35**(2), p 1777–1798. https://doi.org/10.1007/s11665-025-11691-8
19 A. Ali and S.N. Ahmad, Mechanical and Tribological Behavior of TiB2/ Al2O3 Coating on High-Speed Steel Using Electron Beam Deposition, *Tribol. Int.*, 2022, **174**, p 107681. https://doi.org/10.1016/j.triboint.2022.107681
20. S.M. Hashemi, N. Parvin, and Z. Valefi, Effect of Microstructure and Mechanical Properties on Wear Behavior of Plasma-Sprayed Cr_2O_3-YSZ-SiC coatings, *Ceram. Int.*, 2019, **45**(5), p 5284–5296.
21. R.S. Lima, B.M.H. Guerreiro, and M. Aghasibeig, Microstructural Characterization and Room-Temperature Erosion Behavior of as-deposited SPS, EB-PVD and APS YSZ-based TBCs, *J. Therm. Spray Technol.*, 2019, **28**(1–2), p 223–232. https://doi.org/10.1007/s11666-018-0763-6
22. M.A.E. Hafez, S.A. Akila, M.A. Khedr, and A.S. Khalil, Improving Wear Resistance of Plasma-Sprayed Calcia and Magnesia-Stabilized Zirconia Mixed Coating: Roles of Phase Stability and Microstructure, *Sci. Rep.*, 2020, **10**(1), p 1–14. https://doi.org/10.1038/s41598-020-78088-6
23. M. Nejati, M.R. Rahimipour, and I. Mobasherpour, Evaluation of Hot Corrosion Behavior of CSZ, CSZ/Micro Al_2O_3 and CSZ/Nano Al_2O_3 Plasma Sprayed Thermal Barrier Coatings, *Ceram. Int.*, 2014, **40**(3), p 4579–4590. https://doi.org/10.1016/j.ceramint.2013.08.135
24. R. Munisamy, V.G. Umasekar, D. Yogaraj, and S. Sengottaiyan, Effect of High-Temperature Tensile Deformation on the Microstructure, Hardness, Corrosion Resistance, and Wear Behavior of Ti–6Al–7Nb Alloy, *Mater. Chem. Phys.*, 2026, **360**, 132649. https://doi.org/10.1016/j.matchemphys.2026.132649
25. U. Elaiyarasan, V. Satheeshkumar, and C. Senthilkumar, Surface Modification of a Magnesium Alloy by Electrical Discharge Coating with a Powder Metallurgy Electrode, *Mater. Test.*, 2021, **63**(4), p 360–367. https://doi.org/10.1515/mt-2020-0054
26. U. Elaiyarasan, V. Satheeshkumar, and C. Senthilkumar, Effect of Sintered Electrode on Microhardness and Microstructure in Electro Discharge Deposition of Magnesium Alloy, *J. Mech. Behav. Mater.*, 2020, **29**(1), p 69–76. https://doi.org/10.1515/jmbm-2020-0007
27. C. Asokan, U. Elaiyarasan, G. Kavitha, P. Govindhan, and M. Shalini, Development of Empirical Model and Surface Integrity Enhancement of Electro-Discharge Alloyed AA2024 Aluminium Substrate Using a Sintered P/M Electrode, *Can. Metall. Q.*, Taylor & Francis, 2026, p 1–15, https://doi.org/10.1080/00084433.2026.2652158
28. U. Elaiyarasan, P. Baranitharan, V. Satheeshkumar, C. Senthilkumar, and B. Vinod, Wear Behaviour and Coating Performance of WC–Cu Composite Electrodes on ZE41A Magnesium Alloy using Electrospark Deposition, *Can. Metall. Q.*, 2025, **64**(4), p 2114–2127. https://doi.org/10.1080/00084433.2024.2437218
29. U. Elaiyarasan, P. Baranitharan, V. Satheeshkumar, C. Senthilkumar, and T. Arunkumar, Evaluation on Tribological Performance of Ti-6Al-4V Alloy Modified using Powder Composite Electrode-Assisted Electrical Discharge Coating, *JOM*, 2025, **77**(4), p 1834–1843. https://doi.org/10.1007/s11837-024-07070-8
30. A. Dragomirescu, N. Constantin, A. Ştefan, V. Manoliu, and R. Truşca, Advanced Study of Thermal Behaviour of CSZ Comparing with the Classic YSZ Coating, *IOP Conf. Ser. Mater. Sci. Eng.*, 2017, **163**(1)
31. P. Kumaravel, G. Bharathiraja, P. Chandramohan, and S. Mohan, Effect of Oxygen Enrichment in the Emission Characteristics of Yttria Stabilized Zirconia Coated Diesel Engine with Alumina Nanoparticle Additives, *J. Environ. Nanotechnol.*, 2025, **14**(1), p 366–370.
32. A. Tamrakar, V.K. Sahu, S.S. Rajput, P.C. Shukla, and S. Gangopadhyay, Effect of Al_2O_3 Addition on the Characteristics of 8YSZ Thermal

Barrier Coating and its Performance Evaluation in Engine Test, *Ceram. Int.*, 2025, **51**(29PB), p 60786–60800. https://doi.org/10.1016/j.ceramint.2025.10.274
33. A. Ashofteh and S. Seifollahpour, Role of Nano-zones in Enhancing the Performance of YSZ Coatings under Thermal Shock Conditions, *J. Am. Ceram. Soc.*, 2024, **107**(2), p 1201–1218.
34. T. Dharini, P. Kuppusami, N. Kumar, D.D. Kumar, A.K. Soman, and A.M.K. Kirubaharan, Tribological Properties of YSZ and YSZ/Ni-YSZ Nanocomposite Coatings Prepared by Electron Beam Physical Vapour Deposition, *Ceram. Int.*, 2021, **47**(18), p 26010–26018.
35. X. Liu, X. Cao, X. Ma, and M. Li, Surface Characterization of Cylinder Liner-Piston Ring Friction Pairs under Different Temperature and Load by Power Spectral Density Method, *Lubricants*, 2025, **13**(6), p 1–22.
36. J. Wang, J. Wang, Y. Tang, C. Li, Y. Shen, and P.J. Liew, A Study on the Tribological Behavior of the Piston Ring-Cylinder Liner under Ammonia Conditions, *Wear*, 2026, **584**, 206427. https://doi.org/10.1016/j.wear.2025.206427
37. D. Buitkenov, Z. Sagdoldina, A. Nabioldina, and C. Drenda, The study of Tribological Characteristics of YSZ/NiCrAlY Coatings and their Resistance to CMAS at High Temperatures, *Appl. Sci.*, 2025, **15**(14), p 1–15.
38. K. Huo, C. Xu, Z. Huang, J. Xia, L. Zhang, X. Zhang, and T. Li, Effects of Oxygen Gas Flow during Deposition on the Thermal Shock Life of YSZ Thermal Barrier Coatings Prepared by Electron Beam Physical Vapor Deposition, *Coatings*, 2025, **15**(8), p 7–8.
39. P. Banerjee, A. Roy, S. Sen, A. Ghosh, G. Saha, A.H. Seikh, I.A. Alnaser, and M. Ghosh, Service Life Assessment of Yttria Stabilized Zirconia (YSZ) Based Thermal Barrier Coating through Wear Behaviour, *Heliyon*, 2023, **9**(5), e16107. https://doi.org/10.1016/j.heliyon.2023.e16107
40. Z. Gao, G. Ji, Z. Shi, and X. Wang, The Tribocorrosion Behaviour of YSZ Coating Deposited on Stainless Steel Substrate in 3.5 wt.% NaCl Solution, *Ceram. Int.*, 2021, **47**(15), p 21051–21060. https://doi.org/10.1016/j.ceramint.2021.04.107
41. Y. Küçük, Effect of Counterbody on the Dry Sliding Wear Performance of Plasma Sprayed Calcia-Stabilized Zirconia Coating, *Int. J. Refract. Met. Hard Mater.*, 2020, **92**, 105284. https://doi.org/10.1016/j.ijrmhm.2020.105284
42. M.R. Loghman-Estarki, R. Shoja Razavi, H. Edris, S.R. Bakhshi, M. Nejati, and H. Jamali, Comparison of Hot Corrosion Behavior of Nanostructured ScYSZ and YSZ Thermal Barrier Coatings, *Ceram. Int.*, 2016, **42**(6), p 7432–7439. https://doi.org/10.1016/j.ceramint.2016.01.147
43. J. Lin, R. Wei, D.C. Bitsis, and P.M. Lee, Development and Evaluation of Low Friction TiSiCN Nanocomposite Coatings for Piston Ring Applications, *Surf. Coatings Technol.*, 2016, **298**, p 121–131.
44. A. Keyvani, M. Bahamirian, and A. Kobayashi, Effect of Sintering Rate on the Porous Microstructural, Mechanical and Thermomechanical Properties of YSZ and CSZ TBC Coatings Undergoing Thermal Cycling, *J. Alloys Compd.*, 2017, **727**, p 1057–1066. https://doi.org/10.1016/j.jallcom.2017.08.184
45. Z. Rautenbach, M. Haiek, E. Ruales-Carrera, and M. Özcan, Phase Transformation of Yttria-Stabilized Zirconia after the Use of Various Bur Types in Dry and Wet Conditions: A Systematic Review and Meta-Analysis, *J. Mech. Behav. Biomed. Mater.*, 2025, **169**, 107064. https://doi.org/10.1016/j.jmbbm.2025.107064
46. H.Y. Lee, W. Yu, and Y.H. Lee, High-Performance Low-Temperature Solid Oxide Fuel Cell with Nanostructured Lanthanum Strontium Cobaltite/Yttria-Stabilized Zirconia Cathode via Advanced Co-sputtering, *J. Alloys Compd.*, 2024, **972**, 172740. https://doi.org/10.1016/j.jallcom.2023.172740
47. D. Petrescu, A. Nitu, F. Golgovici, I. Demetrescu, and M. Corban, Behaviour Aspects of an EB-PVD Alumina (Al_2O_3) Film with an Interlayer (NiCrAlY) Deposited on AISI 316L Steel Investigated in Liquid Lead, *Metals*, 2023 https://doi.org/10.3390/met13030616
48. C. Uthirapathy and M. Arumugam, Synergistic Effect of Hydroxyapatite and Selenium Coatings on AZ61 Magnesium Alloy for Enhanced Corrosion Resistance and Improved Cell Compatibility in Biomedical Implants, *J. Mater. Eng. Perform.*, 2026 https://doi.org/10.1007/s11665-026-13209-2
49. Uthirapathy Chandrasekaran and Mathivanan Arumugam, Enhanced Corrosion Resistance, Mechanical Stability, and Biocompatibility of AZ61 Magnesium Alloy via Alumina-Selenium Composite Coatings for Biomedical Implant Applications, *Proc. Inst. Mech. Eng. Part L J. Mater. Des. Appl.*, SAGE Publications, 2026, p 14644207251409964, https://doi.org/10.1177/14644207251409965
50. S. Tamil Prabakaran, S. Sengottaiyan, D. Yogaraj, and V.S. Shaisundaram, Multi-scale Optimization and Computational Validation for Enhancing the Microstructure, Mechanical Properties, and Physical Performance of Wire Arc Additive Manufacturing-Fabricated SS309L Stainless Steel, *J. Mater. Eng. Perform.*, 2026, **35**(5), p 4640–4660. https://doi.org/10.1007/s11665-025-11943-7
51. S. Sengottaiyan, S. Subbarayan, R. Natarajan, and V. Gurunathan, Enhancing Mechanical, Degradation, and Tribological Properties of Biocomposites via Treatment and Alumina Content, *J. Reinf. Plast. Compos.*, 2026, **45**(5–6), p 1310–1333.
52. S. Sengottaiyan, Enhanced Mechanical, Dynamic Mechanical Analysis, Thermal, and Tribological Properties of Bio Composites Reinforced with Biosilica from Paddy Straw, *Polym. Compos.*, 2026, **47**, p 7341–7359.
53. A. Kumar, H. Rachwani, and M. Kumar Singh, Dry Sliding Wear Behavior of Hard-Chrome and Zinc-Phosphate Conversion Coatings on Steel Substrates, *Proc. Inst. Mech. Eng. Part J J. Eng. Tribol.*, 2024, **238**(6), p 662–675. https://doi.org/10.1177/13506501241227478
54. C. Ge, X. Ma, H. Li, X. Xu, Z. Peng, Y. Han, X. Lu, and Z. Liu, Evolution of the Tribofilm and Wear State Transition Mechanism of Cylinder Liner and Piston Ring, *Wear*, 2026, **591**, 206616. https://doi.org/10.1016/j.wear.2026.206616
55. M. Nagarajan, C. Gurijala, V.S. Shaisundaram, and S. Sengottaiyan, Assessment of the Microstructural, Mechanical, Corrosion, and Tribological Characteristics of Cold Metal Transfer-Wire Arc Additive Manufactured Al4043 via Response Surface Methodology and XGBoost Machine Learning, *J. Mater. Eng. Perform.*, 2026 https://doi.org/10.1007/s11665-026-13958-0
56 P.C. Huang, C.C. Chou, H.T. Wang, C.H. Cheng, K.H. Hou, and M. Der Ger, Tribocorrosion Study of Electrodeposited Ni[Sbnd]W Alloy/BN(h) Composited Coatings for Piston Rings, *Surf. Coatings Technol.*, 2022, **436**, p 128289. https://doi.org/10.1016/j.surfcoat.2022.128289
57. M. Nagarajan, S. Sengottaiyan, C. Gurijala, and N. Srinivasan, Enhancement of Mechanical, Tribological, and Corrosion Properties of AZ91D Magnesium Alloy Hybrid Composites Reinforced with Al_2O_3 and TiO_2 Nanoparticles for High-Performance Applications, *Ceram. Int.*, 2026, **52**(14), p 26867–26887. https://doi.org/10.1016/j.ceramint.2026.04.238
58. S. P, K. S, S. Sengottaiyan and M. P, Influence of Friction Stir Processing Passes on Microstructure, Mechanical, and Tribological Performance of Al5083/FeCoCrCuTi High-Entropy Alloy Surface Composites, *Compos. Interfaces*, 2026, **33**(2), p 435–460. https://doi.org/10.1080/09276440.2025.2556073
59. K. Kuppusamy, G. Periyappillai, S. Sengottaiyan, and P. Rajendran, Deep Cryogenic Treatment of Various Electrodes for Enhanced Electrochemical Machining Performance of Wire Arc Additive Manufactured Stainless Steel, *Steel Res. Int.*, 2026, **97**(6), p 3339–3356. https://doi.org/10.1002/srin.202501127

Publisher's Note Springer Nature remains neutral with regard to jurisdictional claims in published maps and institutional affiliations.

Springer Nature or its licensor (e.g. a society or other partner) holds exclusive rights to this article under a publishing agreement with the author(s) or other rightsholder(s); author self-archiving of the accepted manuscript version of this article is solely governed by the terms of such publishing agreement and applicable law.